

A Real-time Multimodal Transformer Neural Network-powered Wildfire Forecasting System

Qijun Chen [†], Shaofan Li ^{†1}

[†] *Department of Civil and Environmental Engineering, University of California, Berkeley, California, 94720, USA;*

Abstract

Due to climate change, extreme wildfire has become one of the most dangerous natural hazards to human civilization. Even though, some wildfires may be initially caused by human activity, the spread of wildfires is mainly determined by environmental factors, for example, (1) weather conditions such as temperature, wind direction and intensity, and moisture levels; (2) the amount and types of dry vegetation in a local area, and (3) topographic or local terrain conditions, which affect how much rain an area gets and how fire dynamics will be constrained or facilitated. Thus, to accurately forecast wildfire occurrence has become one of the most urgent and taunting environmental challenges on a global scale. In this work, we developed a real-time Multimodal Transformer Neural Network Machine Learning model that combines several advanced artificial intelligence techniques and statistical methods to practically forecast the occurrence of wildfire at the precise location in real-time, which not only utilizes large-scale data information such as hourly weather forecasting data, but also takes into account small-scale topographical data such as local terrain condition and local vegetation conditions collecting from Google Earth images to determine the probabilities of wildfire occurrence location at small scale as well as their timing synchronized with weather forecast information. By using the wildfire data in the United States from 1992 to 2015 to train the multimodal transformer neural network, it can predict the probabilities of wildfire occurrence according to the real-time weather forecast and the synchronized Google Earth image data to provide the wildfire occurrence probability in any small location ($100m^2$) within 24 hours ahead.

Keywords: Multimodal transformer neural network, Machine learning, Extreme wildfire, Climate change, Convolutional neural network

1. Introduction

Due to climate change, extreme wildfire has become one of the most frequently happening, widely spreading, and most dangerous hazards on Earth. For example, the direct

¹Email:shaofan@berkeley.edu

property damage from the 2025 wildfire in Los Angeles County is estimated at between \$28 billion and \$53.8 billion, according to a report commissioned by the Southern California Leadership Council. Nearly \$150 billion loss in direct damages has been caused by California’s 2018 wildfire alone. In addition, wildfire smoke also causes significant environmental pollution. According to an estimate from a report [1], Global forest fires emitted 5 to 8 billion tonnes of CO_2 each year, and it is more than 10% of the global energy-related CO_2 emission.

In particular, the 2025 wildfire in Los Angeles County have killed at least 29 people, and forced more than 200,000 people to evacuate. While in the 2018 California Camp Fire (see Figure 1 (a)), there were 85 confirmed deaths, 17 injuries, and more than 52,000 people were evacuated. In that fire, more than 18,804 building structures were destroyed, and the burn area exceeded 621 km^2 . The Camp Fire caused more than 16.65 billion dollars in direct damage alone (2018 USD)). Figure 1 (b) shows the geographical distribution of the wildfire that occurred in the United States.

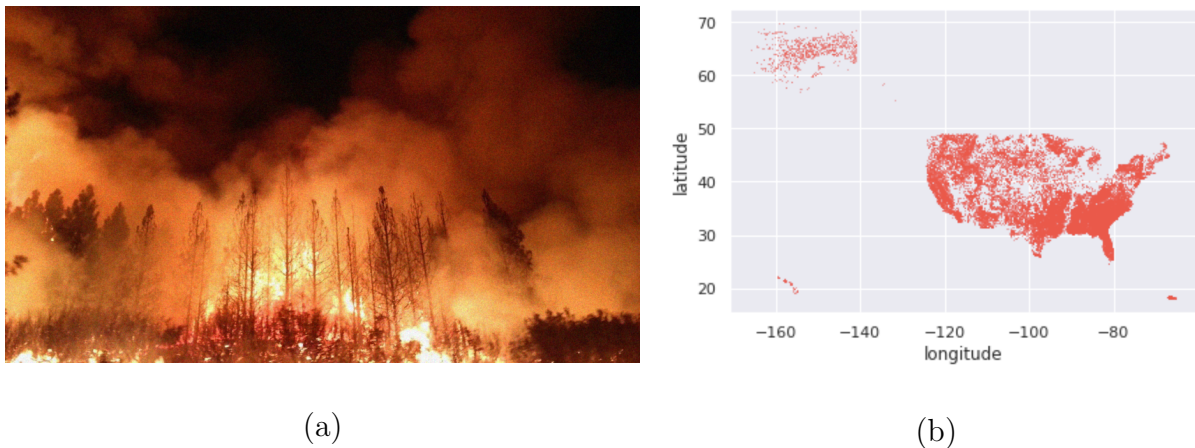


Figure 1: (a) 2018 California Camp Fire [Photo: U.S. Department of Agriculture/Wikimedia Commons], and (b) Geographical locations of wildfires occurred in the United States

By accurately forecasting the wildfire occurrence location and its timing, we cannot only reduce the indiscriminate power shutdown in the fire season, which causes power outages resulting of closing businesses and schools, but also allow us to take active specific and direct preventive measures in surgical precision. For instance, if we know the precise fine-scale fire occurrence location, we can control the vegetation growth and state in the specific predicted location in a relatively short time with low cost and high efficiency.

Since the 2010s, several studies have used artificial intelligence-related or machine learning (ML) based methods to predict wildfire occurrences in a relatively large area e.g. [2, 3]. However, most of these research works are still at a scholarly research level but not at the practical fire-hazard prevention stage, such as forecast the precise occurrence location within 1 mile radial distance.

The current ML-based wildfire prediction models used the existing wildfire data and large-scale weather data to predict possible fire locations. Even though the existing machine-

learning neural network models may be able to predict some fire occurrences, the predicted location is inside a large area ($> 10 \text{ mile}^2$). However, the actual and precise wildfire occurrence location in a landscape is strongly influenced by local weather, terrain, and vegetation conditions. Precisely speaking, the precise fire occurrence location depends on the small-scale weather, terrain, and vegetation conditions that cannot be obtained from the existing database or weather forecasting, but can only be extrapolated or correlated with the local terrain and vegetation conditions, and some of them can only be represented by the spatial conditional probability distribution.

Moreover, in some advanced studies on machine learning-based wildfire occurrence predictions, most researchers adopt the logistic regression statistical analysis (correlation) and artificial neural network (ANN) approach to directly predict fire occurrence by adding vegetation cover[4], slope, elevation, the density of livestock, precipitation conditions, and lightning polarity as features (See: [5, 6, 7]). However, the spatial scale of these features is either inconsistent with the scale of weather forecasts or incompatible with the length scale of the existing wildfire data.

Since wildfire occurrence and its severity in a landscape is strongly influenced by both weather and terrain conditions [8] at different locations, and in different spatial and temporal scales, By categorizing the different causes of wildfire, and using and learning from the vast wildfire data, in this work, we are developing a multiscale multimodal learning neural network model that can provide the conditional probability of the wildfire for different causes,

Unlike the current straightforward and elementary machine learning approach, the proposed Machine Learning Neural Network approach can offer an efficient tool to practically forecast the probability of wildfire occurrence in a small-scale spatial location and a precise time frame. It not only takes into account large-scale regular weather and historic wildfire data such as hourly weather forecasting data, but also utilizes small-scale geographic information such as local terrain conditions and local vegetation conditions extrapolated from Google Earth images to obtain the probabilities of wildfire occurrence with respect to small-scale location as well as their timing.

2. Data Collections and Data Pre-processing

In this work, the wildfire data collected are only within the United States to demonstrate the feasibility of the developed machine learning neural network.

As shown in Figure 2, the wildfire data is mainly consists of two parts. The first part is the information data, and the second part is the imagery data. Within the first part, information data is a combination of three categories or sets of data: wildfire information set, weather information set, and vegetation information set. The first data set is wildfire information, which consists of geo-referenced wildfire records from the United States Department of Agriculture (USDA) [9] from 1992 to 2015 of 24 years,

The geo-referenced records mainly include the fire location, which is latitude and longitude, the size of the fire, which is treated as quantitative data, and the causes of fire including the date of the wildfire, which is also qualitative data.

In this study, the qualitative data will be converted into quantitative data by using methods such as One-Hot Encoding [10]. The miscellaneous data such as the fire name, and the fire ID are not included in this class of data. The second data set, weather information, contains mainly Integrated Surface Data (ISD). It contains the records of the weather conditions before the wildfire occurred. For instance, it may contain the 7 days hourly average temperature before the discovery date in the wildfire records. The vegetation information will contain the categories of the location that wildfire was occurred in the wildfire records. The second part is the imagery set that is manually obtained by software such as Google Earth Pro[11]. It contains the obtainable images at the specific time when the fire occurred within a certain radius from the fire locations as the center with a clear view of the surface situations.

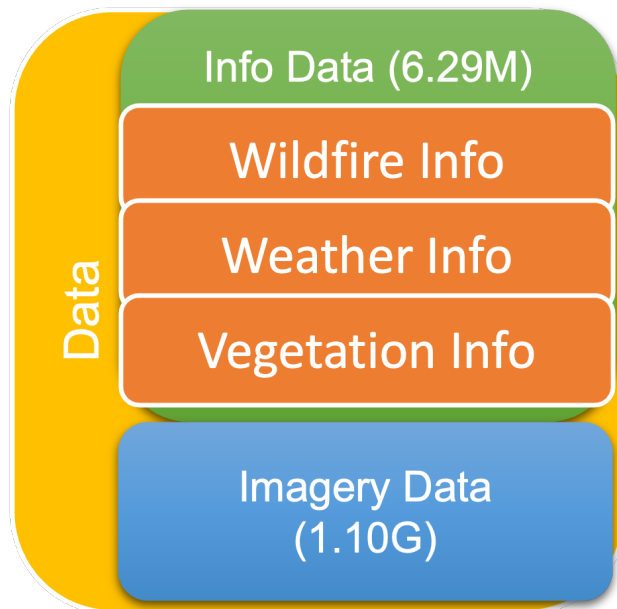


Figure 2: Data Components

Since some data may not be available when combining two parts, we remove the data with missing values.

2.1. Information Data

The information data refers to the general information of a wildfire, and it mainly consists of three parts: wildfire records, the associated weather information, and the local vegetation information.

In this work, the wildfire data records are obtained from the Fire-Occurrence Database, FPA_FOD, and the data used in this work contains spatial wildfire occurrence data for the United States from 1992-2015. Since this database is kept renewed, currently, the FPA_FOD database has all the data collected from USDA from 1992-2022 [9]. This wildfire database has its special data format, such as Object_ID, Source_SYSTEM ID, Report agency ID,

LOCAL_FIRE record ID, etc. (see Figure 5). When extrapolating the wildfire data from the database, the essential information is maintained, which includes the latitude of the fire occurrence location, the longitude of the fire location, which is at least with the precision as required in Public Land Survey System (PLSS) [9], the size of the fire, the cause of the fire, date when the fire was discovered.

The next set of information data is the hourly weather data, which is obtained from the National Centers for Environmental Information (NCEI) database that uses the nearest NOAA station[12] based on the latitude and longitude from previous information databases. The hourly weather data includes average temperature, wind speed, humidity, and precipitation in $^{\circ}C$, m/s , $\%$, and mm separately at the location of the wildfire mentioned above up to 30, 15, and 7 days before the discovery of the wildfire. Since the recorded time from *FPA_FOD* is the discovery time, getting the exact time is difficult, in order to reduce the inaccuracy from the records, the average information will be applied. For example, we take the average of $avg(30 \times 24)$, $avg(15 \times 24)$, and $avg(7 \times 24)$ and keep three numbers as its temperature value.

The vegetation information contains the vegetation categories of the location where the fire occurred. It is available at OPeNDAP[13] dataset, a remote data retrieval software. For example, for the case of fire, as shown in a Google Map capture in Figure 3, caused by lightning occurred at location $(35.7044444N, -118.5883333W)$ in date 8/18/2013, which is in Florida, and it has a fire size of 76, and the average temperature, wind, humidity, and precipitation data before the fire occurrence date in 7, 15, 30 days, and the vegetation type is characterized as the shrubland type, or shrubland.

The original data from *FPA_FOD* for fire information has 1.88 million entries. It is an enormous amount of data and not all of the entries can obtain enough information such as weather or vegetation. We also combined with a exist data that is available from GitHub for the information set[14]. Currently, with the combined part, the total amount of data obtainable is about 29550. Figure 1 shows the plot of latitude and longitude from the current data for all fire cases and time. The information data itself can also be used to train the baseline model. Since in this work the model’s neural network architecture has been developed, in the future, once the new data become available, we will generate new data and feed them into the model.

2.2. Imagery Data

The second part of the data are the images of the locations, and this part of the data contains all the known wildfire location images that was captured by Google Earth Pro[11]. Google Earth Pro provides satellite images for each location, however, these images are not captured continuously. For instance, the time when some images are taken in the same location may have a several-month time difference. Moreover, the obtainable images may not be the exact date when a fire occurred. Within the data set, the image adopted will be the first available image before the wildfire discovery date (*disc_date_pre*).

Moreover, the image qualities in different pictures are also different due to the different cameras on different satellites used taking those pictures, or due to other causes such as different sunlight or cloud conditions. These images were taken by the cameras or sensors

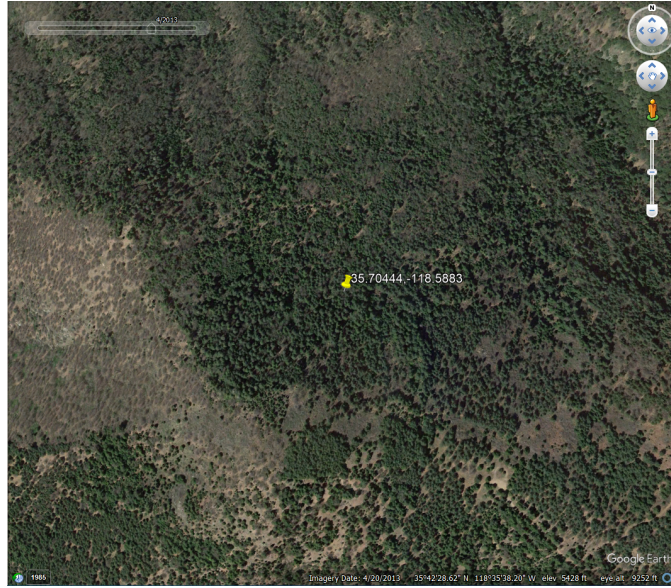


Figure 3: An example of image file from Google Map @35.7044,-118.5883333, on 8/18/2013

from multiple satellites such as Landsat, NASA satellite [15], or Sentinel satellites from ESA[16] at different times with different sensor technologies. For example, the most recent United States Geological Survey (USGS) Landsat 9 has ultra blue (coastal aerosol) surface reflectance for Band 1, which allows for coastal watercolor observation, and Band 2, 3, and 4 surface reflectance are blue, green, and red. However, some images were taken by using USGS Landsat 7 that only have blue, green, and red bands. Therefore, the quality may vary due to the improvement of satellite and sensor technologies. Furthermore, since the data were taken in 24 years, most images obtained in the 1990s are black-white grayscale images. This can be seen from image number 5536 in Figure 4, and some images may be also in poor quality due to the glare or sunshine, such as the number 11191 image taken from the satellite as shown in Figure 4. But after 2005, with the advance in satellite image technologies, the image quality is much better than those images taken before. Table 1 shows some basic settings when the images are captured from Google Earth Pro. Turning the setting sun off will result in a mask alleviating the effects of the sun, which can also help keep the consistency of the image quality. In Google Earth Engine[11], it automatically masks the clouds if the cloud is in the satellite image, thus, one can obtain ground images without clouds by unchecking the cloud in the settings. The map scale is in default for Google Earth Pro, when the images are being processed and it will crop and re-scale the size of the images. The road or any other irrelevant marks or pins are also removed when capturing the images. Thus, as shown in Figure 4, the images taken from Google Earth Pro are purely terrain-type without any pins or marks.

To efficiently generate data, automated software is used to generate the image data. With the help of Pulover’s Marco Creator[17], a software that can automate simple mouse clicks and complex macros with loops and conditions[17] is used, which can automatically capture the images from Google Earth Pro. This software can record the action that one makes, then

Parameters	Value
Scale	1:1000
Historic imagery	on
Terrain	on
Cloud	off
Atmosphere	off
Sun	off

Table 1: Settings for Google Earth Pro

repeat the process until a certain amount of images are obtained. In this work, we installed the software and Google Earth Pro in a Dell Precision Tower 5820 desktop, and we collected all image data in almost three months. After we gathered the images, we cropped and scaled the images into the size or scale that desired, which is H: 100 *pixels* \times W: 100 *pixels* within the approximate length of 100 meters by 100 meters where the center is the coordinate of the wildfire occurred.

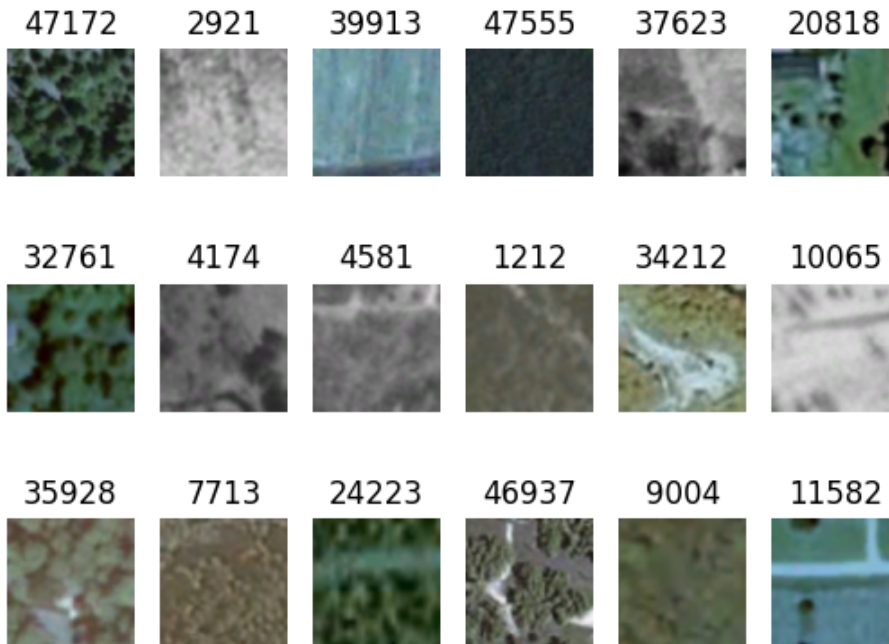


Figure 4: Images randomly chosen from the image dataset, and the indices of the images is on top, each image is in 100 *pixels* \times 100 *pixels* (Height \times Width)

To obtain 1.88 million images from Google Earth is time-consuming even using automation software. Each image entry may take more than half a minute to finish, not including time delay caused by other reasons such as data requesting and data fetching. Sometimes, some locations do not have satellite images, which will lead the computer to pause because of the incorrect date format due to the software’s default settings.

2.3. Data Pre-processing

To maintain the consistency of image data information and avoid poor contrast, when handling the image data, the data were transformed and normalized [18] all the images to gray-scaled to keep consistency with the low contrast images, and it will be normalized the image data before training them by dividing the gray-scaled image data by 255. After the process, these two data sets are concatenated by the accordance index and generate a new data set including the weather data, vegetation, and processed satellite images from the map. Therefore, the ready-to-train data set has a dimension of 29550 rows and 21 columns plus the image features.

Before training, the data were split into three subsets, the first one is temperature and wind, then the second subset includes two more features: humidity and precipitation. In the third subset, vegetation categories are included to evaluate the performance of the baseline models with different features. Our current target is to predict the probability of whether a certain natural condition will cause wildfire at certain locations, for instance lightning, as a main ignition source of natural wildfire [19]. Even though some wildfire machine learning models in the literature also claim to be able to predict human-caused fire occurrence, e.g. [20], predicting human-caused wildfire is not the objective of the present work.

Other causes shown in 5 are also directly or partially directly caused by humanities, for now, it is hard to predict them because they are based on human behaviors [21], whose statistical information is not clear. While the cause of power line may not be caused by human activities[22], thus in the data description one can see that the relative frequency of wildfire caused by power lines has an extremely small amount compared to that of other causes, as shown from Figure 6 (a). For this perspective, as shown in Figure .10, one can treat this problem as a classification problem. Thus, for predicting wildfires caused by nature, lightning can be used as a label. However, the proportion of the label as lightning has about 4717 cases among 29550, as shown in Figure 6 (a), which is only about 15.96% of the entire data. From Figure 6 (b) that the data points are much more sparse compared to the entire data point in Figure 1 (b), which may lead the data imbalanced [23]. Since about 84% of the binary label is false, and it will have a significant effect on the prediction results, which the model will tend to have more false in results instead of true, which can lead to a low true positive rate, because identifying all false will lead to an average 84% accuracy. Thus, a re-sampling method could resolve this issue, which will be discussed in the subsection follows.

2.3.1. Data Resampling

There are several data re-sampling methods, e.g. undersampling[23], oversampling or SMOTE[24]. In the proposed model, two methods are applied: One is Synthetic Minority, an oversampling technique (SMOTE)[24], that increases minority by analyzing the minority population and generate new samples to increase the amount instead of simply copying the sample to data, which may cause an overfitting problem (see 5).

The other method used is the undersampling[23] method. This method simply decreases the proportions of the majorities by deleting occurrences of the more frequent class. It can balance uneven datasets by keeping all of the data in the minority class and decreasing

the size of the majority class[23]. Nevertheless, it may decrease the train data size. In the present work, this method is used by randomly choosing a certain amount of data from majorities and combining them with the minority to adjust the proportion. By putting the extra majorities to the test case, these methods increase the size of the test cases. However, it helps us check the performance of the model, since most of the data are not being trained, and test data are even larger than train data. Therefore, between these two methods, we favor the undersampling approach. Thus, re-sampling the amount of the minority data to a certain level, say, the odds can be 1 : 1.8, which is about 35.72% as shown in Figure 5 is an optimal choice.

Therefore, we randomly choose data from non-natural causes, then combine it with 4717 nature-caused wildfire data to keep the proportion as 35.72%. If we set the proportion to 1 : 1, which is 50% for the training and the test data, it will lead to a very small training data set with 7547 data trained and a larger test set. Thus, we prefer an optimal solution of setting the proportion. Through this method, the test set will be relatively large compared even to the train set, it can help us test the model performance better.

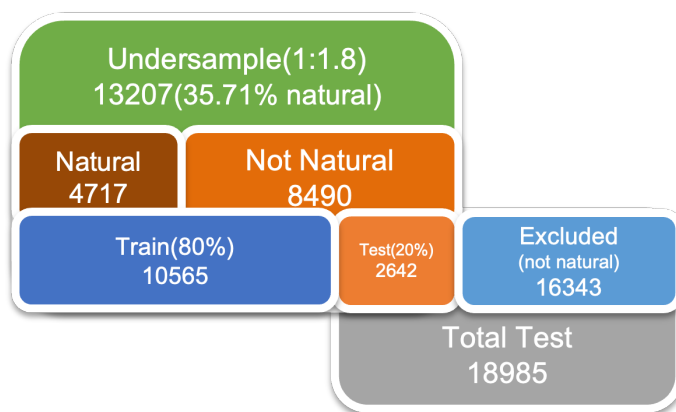


Figure 5: Data split detail, Total 29550, naturally caused 4717, non-natural caused 8490, train size 10565, test size 2642, total test 18985

Nevertheless, this may decrease the training data size. In the present work, we apply the method by randomly choosing a certain amount of data from majorities and combine them with the minority to adjust the proportion. We will put the extra majorities to the test case and increase the size of test case. This will lead a large amount of test cases, however, it actually helps us checking the performance of the model, since most of the data are not being trained, and test data are even large than train data. Therefore, between these two methods, we favor the undersampling approach. Thus, we re-sample the amount of the minority data to a certain level, say, the odds can be 1 : 1.8, which is about 35.72% as shown in Figure 5.

Before training, the data will be first split into two sets: the training set and the test set. If the proportion of the total data is about 80% of the training set and 20% test set, it will have a total of 10565 in the training set. Based on this setting, the rest of the non-natural causes data will all be in the test set which leads to $2642 + 16343 = 18985$ test cases. For

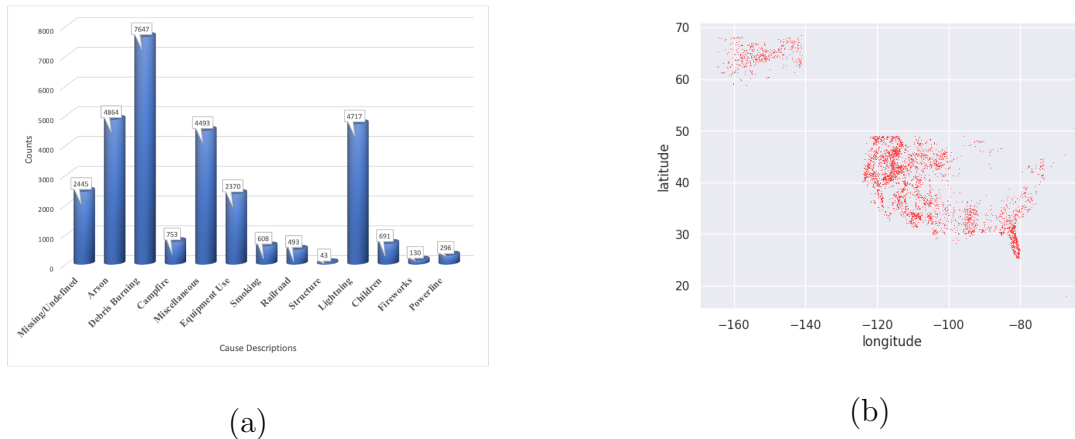


Figure 6: (a) Histogram of different wildfire causes, and (b) Natural caused (lightning) wildfire distributions.

the training purpose alone, a small size training data set may not be good, however, a larger test size can provide more plausible results. This method also helps to check whether the model is overfitted during training. Most of the non-natural causes are not included in the model during training using undersampling. When testing the model, these cases are the model never seen during training. Thus, if the model still performs well during testing, the model is not affected by the proportion, and it will not be overfitted.

2.4. Data Uncertainties

In data processing and characterization, we assume that all the data provided by the source is accurate enough including the images from Google Earth Engine. It contains less epistemic uncertainty, if any. In reality, however, this may not be the case.

In general, outliers may not affect the machine learning training results, however, some data features that have significantly large error may affect the training results. For instance, in the first part of the data, the weather condition information at a specific location may be recorded from the nearest National Weather Service Station (NWS) or the nearest National Oceanic and Atmospheric Administration (NOAA) station, while some stations may be far away from the location, Thus, some of the weather information may not be accurate. Moreover, the date and time when the fire was discovered may also not be accurate. Wildfire is a complex process and its occurrence is the product of several interrelated factors, including ignition source, fuel composition, weather, and terrain topography feature [25]. When a fire starts, especially for those nature-caused fires, it may take a while for people to find or discover them, if the fire is far away from society. Under those circumstances, the causes of the fires may also be hard to find out, therefore, some causes may also not be accurate.

As mentioned in Section 2.2, the qualities of the images are varied due to the technologies. Another assumption is also made that the area before a wildfire occurred may not change a lot during that period. The images are stitched from Google Earth Engine, and all pieces of an image are not consequently captured by satellites at the same time. Some images taken even have several years difference, for example, the last image for a certain location may be captured two years ago. Furthermore, the season when the images are being taken may also

affect the results. Based on the observation of the images, satellite images do not provide normal qualities of some locations such as some place in Alaska or some places that hardly have people, which means that the image has quite low resolution, and some images only appeared with less color spectrum without showing the exact terrain. Therefore, the quality of image data still needs to improve.

Moreover, the data used in this work only contain the data of the wildfire that had occurred inside the United States. Thus, based these data, the prediction of the wildfire occurrence outside the U.S. may not be accurate.

2.5. Data and Code Availability

It is both preferable and sustainable to feed more data to train the AI model to obtain better results. All training data can be found on the official websites, and imagery data is also available on 5. The computer codes for generating visualization are available on Colab. See 5 for the ReadMe and instructions.

3. Methods

3.1. Statistical Settings

The technical objective of this work is to predict whether a location is at risk of wildfire occurrence. The prediction is characterized by a set of conditions, natural or man-made. Mathematically, this prediction may be expressed in terms of conditional probability defined as follows,

$$\mathbb{P}(\textit{wildfire}|\textit{natural causes, other conditions}) \quad (1)$$

In our data format, all the data entries are related to the wildfires that have been actually occurred. By virtue of probability chain rule, the condition probability of a wildfire occurrent due to natural causes, or other conditions can be expressed as follows,

$$\begin{aligned} & \mathbb{P}(\textit{natural causes}|\textit{wildfire, other conditions}) \\ = & \frac{\mathbb{P}(\textit{wildfire, natural causes, other conditions})}{\mathbb{P}(\textit{wildfire, other conditions})}, \end{aligned} \quad (2)$$

Finally, we can reformulate Eq. (1) by using Bayes' Theorem,

$$\begin{aligned} & \mathbb{P}(\textit{wildfire}|\textit{natural causes, other conditions}) = \\ & \frac{\mathbb{P}(\textit{natural causes}|\textit{wildfire, other conditions})\mathbb{P}(\textit{wildfire, other conditions})}{\mathbb{P}(\textit{natural causes, other conditions})} = \\ & \frac{\mathbb{P}(\textit{natural causes}|\textit{wildfire, other conditions})\mathbb{P}(\textit{wildfire}|\textit{other conditions})\mathbb{P}(\textit{other conditions})}{\mathbb{P}(\textit{natural causes, other conditions})} \end{aligned} \quad (3)$$

When we are modeling for $\mathbb{P}(\textit{natural causes}|\textit{wildfire, other conditions})$, we assume that the location has had a wildfire and try to identify the conditional probability of its cause.

Among these probabilities, the probabilities, $\mathbb{P}(\textit{natural causes}, \textit{other conditions})$ and $\mathbb{P}(\textit{other conditions})$ shown in Eq. (3), can be predicted by other sources such as weather forecasts. Then based on the prediction of weather forecast, we can obtain the probabilities due to natural causes, i.e. the probabilities of storm weather in a certain area. For the $\mathbb{P}(\textit{wildfire}|\textit{other conditions})$, we can refer from Probability of Ignition[26] provided by NWCG. Instead of directly predicting the conditional probability, our model will focus on the prediction of the likelihood probability of the natural causes given the occurrence of wildfire, for instance, the lightning caused wildfire, which can be directly found in the data. Thus, once we know three of them, we can have all the probability needed to make a posterior prediction.

Furthermore, based on Eq. (3), we have

$$\begin{aligned} & \mathbb{P}(\textit{wildfire}|\textit{natural causes}, \textit{other conditions}) \\ & \propto \mathbb{P}(\textit{natural causes}|\textit{wildfire}, \textit{other conditions}), \end{aligned}$$

Thus if one of the probabilities increases the other one will act the same, and we can choose one to represent the other.

Figure 7 is a flowchart that outlines data flow for the proposed model discussed in the previous Section. For each past wildfire record, we collected the weather, location, date, vegetation, and image data based on the given location and date. For the information data without images, which is the features associated with locations, weather, and vegetation categories, we process the data directly to a neural network[27]. Then our model without images can also provide predicted probabilities as outputs. To validate the correctness of the proposed model, we defined a classification threshold, 0.5. Thus, if the probability is less than the threshold, we categorize it as false otherwise 1. With these metrics, we can assess the accuracy of the proposed model. For the data with images, inspired by architectures of CNN[28], ResNet[29], and Transformer[30], we designed and implemented a feature extraction model that consists of a light version of ResNet with a modified ViT[31] with image features to exaggerate the features that it can discern but humans cannot see by naked eyes and with as much low computation cost as possible. By doing so, we can then output some new features to predict the risks of wildfire at certain locations.

Moreover, to have a stable results, the model will first find the mean of two probabilities and then predict the probabilities in Eq. (2). To quantify the probabilities, the confusion matrix is used to determine whether the results predicted by the model are accurate or not.

As shown from Figure 7, all the features in information data and image data are based on the location and weather conditions. Hence, with some feature selections, a designed model is used to extract and enlarge the image features, so that we can predict the probabilities such as

$$\mathbb{P}(\textit{wildfire}|\textit{natural causes}, \textit{other conditions})$$

For the given location and weather information, the transformer machine learning model can obtain the data from the sources and calculate the probabilities. If the probabilities are larger than the threshold that we set, we can then say that if a given natural cause

occurs the fire should occur under the circumstance of the weather and vegetation/terrain conditions. Otherwise, the fire will not occur.

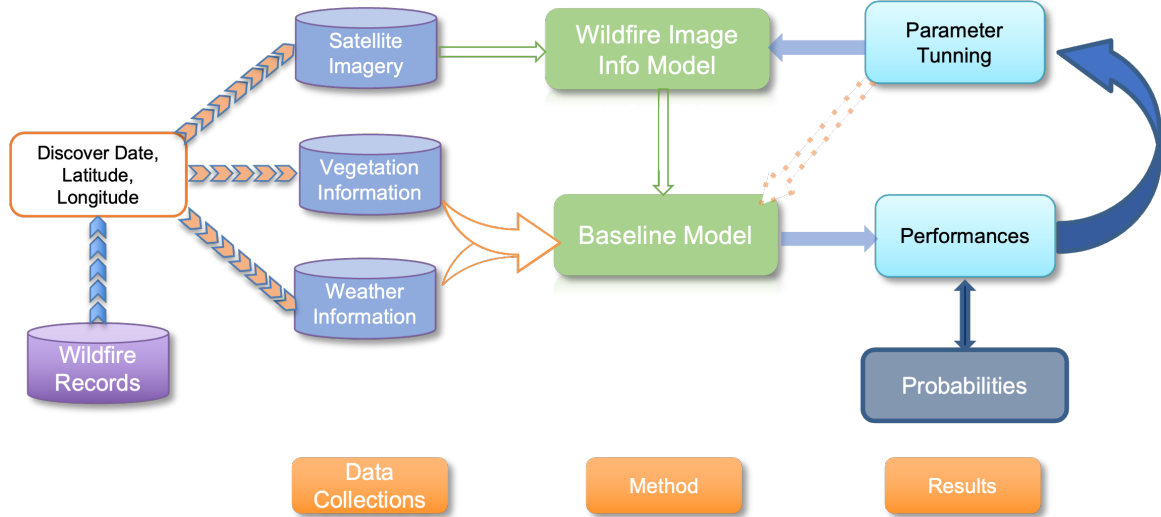


Figure 7: Overview of Data Flow in Model

3.2. Baseline Model

In the first phase of the training, the baseline model used is a deep learning neural network[32], in which only the information data is used to illustrate how new features would affect the results. We used several different combinations of features to observe the result or output variations, which include temperature plus wind, temperature plus wind plus humidity plus precipitation, temperature plus wind plus humidity plus precipitation plus hot-encoded vegetation, etc. First, only geo-referenced records would be fed into the model. Both the classification method and regression method are used to predict the probability results. Since in this case, one would like to have a probability result and the regression strategy can provide better and more stable results, thus, regression strategy is used for the task, and the results shall be discussed in the next section.

For this neural network architecture, the model has five fully connected hidden layers, and each layer can be treated as a block. As shown in Figure 8, after the input layer, each of these consists of two or three parts, hidden layer, batch normalization layer [33]. Here, the activation function is rectified linear unit (ReLU)[34], while the last layer is another fully connected layer. Inside this model, the total amount of variables is 49705.

From the batch normalization algorithm, through a linear combination, the mean and standard deviation of each input for the block will be within a certain range, so that the next layer does not need to satisfy the changes and increase the efficiency of the model[35]. Moreover, the model will depend less on hyper-parameter tuning so that it allows a little larger learning rate. It will also shrink the internal covariance shift[33].

From the batch normalization algorithm, we can see that through a linear combinations, the mean and standard deviation of each input for the block will be within a certain range,

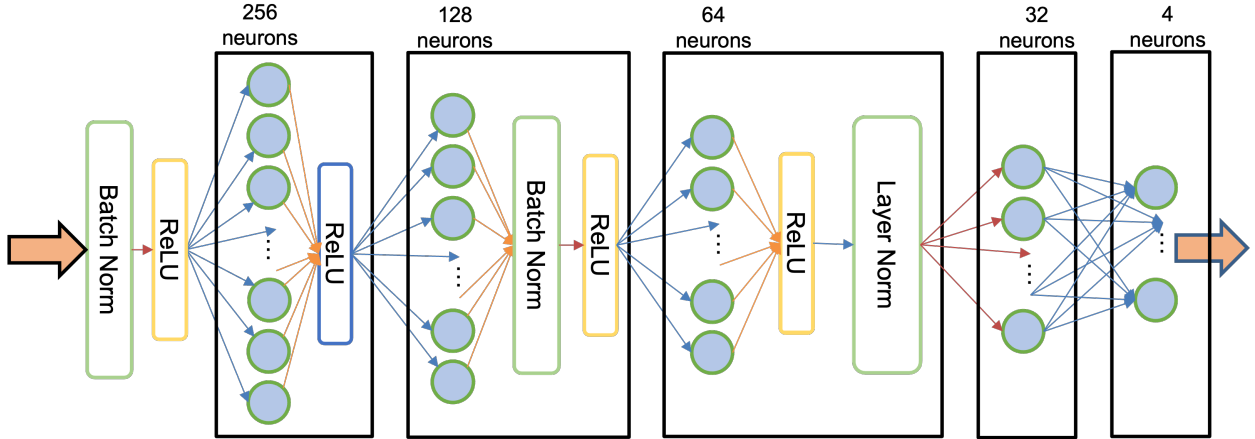


Figure 8: The architecture of the proposed machine learning model as a hybrid deep neural network.

so that the next layer does not need to be adjusted with possible changes and increase the efficiency of the model[35]. Moreover, the model will depend less on hyper-parameter tuning so that it allows a little larger learning rate. It will also shrink the internal covariance shift[33].

Since we do not use batches in this model, the batch norm layer will be simply the normalization of the entire input matrices. With the same architecture shown in Figure 8, we appended vegetation categories and trained the model again.

Inside the model, as shown in Table 2, the loss function we use is the mean square error (MSE), which is a widely used loss function, and the Cross Entropy loss[36] is also available in the code for classification.

$$MSE = \frac{\sum_{i=1}^n (y_i - \hat{y}_i)^2}{n} \quad (4)$$

where n is total amount of data, y_i is the i th true label, and \hat{y}_i is the i th predicted label by model. This metric provides an intuitive difference between the true values and the predicted values.

Another way is treating the model as a classification problem. Thus in the model, the loss function can be the Cross-Entropy loss function [37], which requires one-hot encoding of the label and changing the layer in the baseline model to SoftMax[38]. A new loss function called true rate loss will calculate both sensitivity and specificity are defined, and then maximized it. For finding the gradient, the Adam optimizer[39] is used.

Training this model does not necessarily need a local GPU and large RAMs. It would only take about several seconds for 100 epochs without a mini-batch by using a standard NVIDIA T4 Tensor Core GPU with 16G RAM on Google Colabotory[40], where the codes and pre-trained models are also available on given Colab. For a single CPU training without a mini-batch method, it will also only take less than 30 seconds.

Parameters	Values
Hidden Layers	[256, 128, 64, 32, 4]
Loss Function	Mean Square Error (Cross Entropy)
Optimizer	Adam optimizer[39]
Learning Rate	0.01
Weight Decay	1e-4
Epochs	100
Batch Size	NA

Table 2: Hyperparameters for Neural Network

3.3. Wildfire Imagery Information Net (WIIN)

Besides the information data, for the imagery data collected, we designed a Wildfire Image Information Net, which can extract the features from the images according to our purpose. It is a combination of a deep learning architecture of ResNet[29] type and a transformer with an attention-based architecture.

Initially, a transformer is used in translation for the natural language process, thus, the self-attention mechanism focuses more on the locations of a word and its score in a given sentence, which is beneficial for understanding complex language structures.

When applying the transformer to images, a conventional vision transformer focuses on classification or segmentation. It represents the information by token features, which are also known as class features. However, our model is not concerned with classification but only interested in the information embedded in images, Therefore, the proposed model focuses more on what has been “told” by an image.

To make this work for the abandoned image pixels from the conventional vision transformer, the model not only applies the self-attention mechanism but also adds a convolutional block to process the image pixels through a multilayer perceptron so that the model can extract image features from it as shown in Figure 9.

The reason why the ResNet is applied before the transformer[30] is because usually, a transformer requires a large amount of data[41]. However, in our case, instead of using a large amount of data like GPTs[42] are using, we have limited training data size, after the undersampling method is applied, we only have about 10000 data for training. Thus, in order for the transformer can have better performance in image processing, we enlarge the features by using ResNet. ResNet has CNN-like[28] architecture, it can extract the feature maps from the original image[43], which would make it easier for a transformer to process the feature maps instead of the original images. Moreover, based on its architecture, a transformer with attention mechanisms will act as an encoder to analyze these images. After embedding an image, it can assign the scores and find the most possible patches that are related to the target. As shown in Figure 9, we split the output features into two parts: the token feature and the image feature. Both features will append to the information data as new features and feed into a deep neural network for training. Thus, with the original 21 features, there are a total of 23 features when using the combined model.

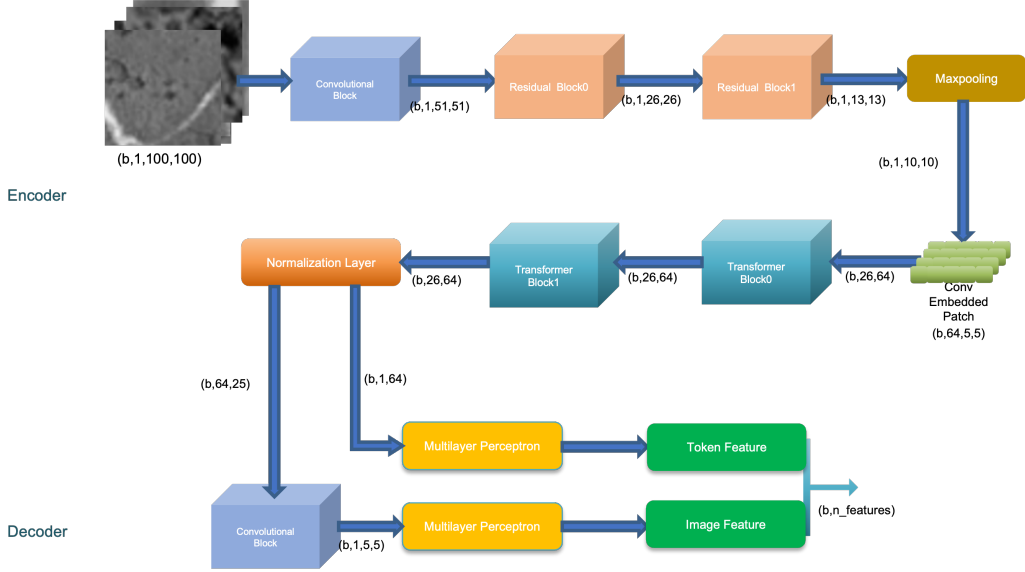


Figure 9: Architecture of Wildfire Imageries Information Net (WIIN) (b:batch size)

3.3.1. Residual Network

At this stage, feature maps from the original captured image are extracted so that the model can both maintain its performance and save computation power. As shown from Figure 9, the mini-batched images with the size of (100, 100) will first go through a convolutional block, which includes a convolutional layer, a batch normalization layer, an activation layer, and a max-pooling layer, as shown on the left of Figure 10 (a). The convolutional layers are used to extract features from any previous procedures, and it will output a new feature map of the previous stage of an image or feature map [43]. Mathematically, for a grey-scaled image $I \in \mathbb{R}^{W \times H \times 1}$, where W stands for the width of the image, and H is the height of the image, the ij -th entry of output feature map by using the kernel $K \in \mathbb{R}^{p \times q}$ can be represented as [44]

$$\sum_i \sum_j K_{(i,j)} I_{(p-i,q-j)}$$

In this stage, the convolutional layer has a kernel size of 5, stride of 2, and padding of 3. Taking Figure 10 (b) as an example, the blackboxes with 0s are the padding area, and the rest are pixels of the original image. The 5×5 yellow and green shaded areas will multiply weighted kernels that will be trained at different times, and each time, the kernel will move two boxes since the stride is set to 2.

Similar to the convolutional layer, the maxpooling layer will keep the main features and reduce parameters in the model, it removes all the values except for the maximum value in each filter process [43]. It will then obtain the maximum numbers within each kernel instead of multiplying the trained weights. Therefore, after the convolutional block, the image size will become (51, 51) as unnecessary features would be removed.

Then, the convoluted images will be fed into two residual blocks with three and two layers separately. The residual blocks are mainly two convolutional blocks without the max-pooling

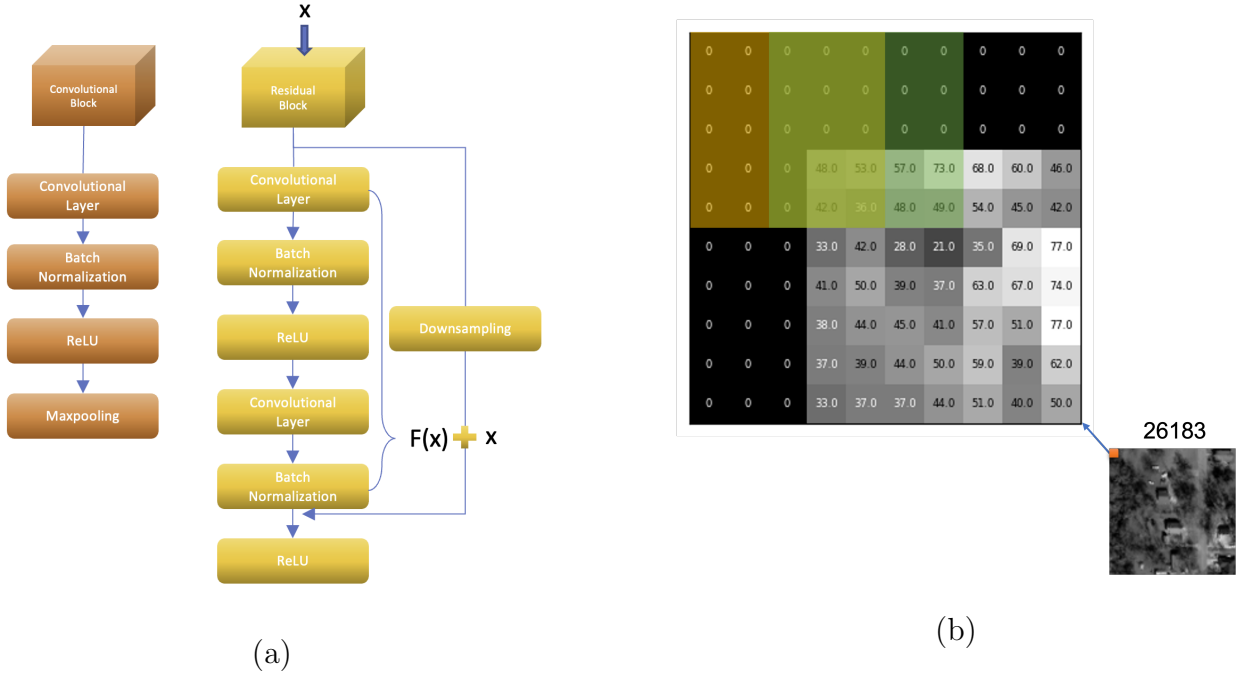


Figure 10: (a) Convolutional Block; RIGHT: Residual Block, and (b) Top left corner of image 26183 in the first convolutional layer with kernel 5×5 , stride 2, padding 3.

layer, added with downsampled initial inputs as residuals if necessary. As shown in right of Figure 10 (a), for a single residual block, the new residual $F(x)$ will add back to initial input value x to create a new output $F(x) + x$. With the help of adding residuals to the output, ResNet can provide a good feature map from the original image without losing too much information and prevent the gradient vanish or exploding [45, 29]. Even if the fed data has a small image size, it works well. After two residual blocks, the image size reduces to (13, 13), and we then feed the processed images into the last max-pooling layer. Mathematically, let $F(\cdot) = BN(Conv(\cdot))$ Similar to the convolutional layer, the max-pooling layer will keep the main features and reduce parameters in the model, it removes all the values except for the maximum value in each filter process [43]. It will then obtain the maximum numbers within each kernel instead of multiplying the trained weights. Therefore, after the convolutional block, the image size will become (51, 51) as unnecessary features would be removed.

Then, the convoluted images will be fed into two residual blocks with three and two layers separately. The residual blocks are mainly two convolutional blocks without the max-pooling layer, added with downsampled initial inputs as residuals if necessary. As shown in right of Figure 10 (a), for a single residual block, the new residual $F(x)$ will add back to initial input value x to create a new output $F(x) + x$. With the help of adding residuals to the output, ResNet can provide a good feature map from the original image without losing too much information and prevent the gradient vanish or exploding [45, 29]. Even if the fed data has a small image size, it works well. After two residual blocks, the image size reduces to (13, 13), and we then feed the processed images into the last max-pooling layer.

Mathematically, let $F(\cdot) = BN(Conv(\cdot))$

$$\begin{aligned}
z_0 &= F(x) \\
z_0 &= \text{maxpool}(g(z_0)) \\
z'_i &= F(g(z_{i-1})) \\
z_i &= g(F(z'_i) + z_{i-1}) \\
z_i &= z_i + \sum_{i=1}^{L-1} F(z_i) \\
y &= \text{maxpool}(z_i)
\end{aligned}$$

where BN stands for the batch normalization layer, $Conv$ is the convolutional layer, maxpool is the maxpooling layer, and $g(\cdot)$ is the activation function.

Parameters	Values
Layer(Kernel, Stride, Padding)	conv(5,2,3); maxpool(3,2,1); conv(3,1,1)+conv(3,1,1) \times 3; conv(3,2,1)+conv(3,2,1) \times 2; maxpool(4,1,0)
Epochs	300
Batch Size	32

Table 3: Hyperparameters for ResNet

3.3.2. Wildfire Images Transformer (WIT)

In the transformer stage, similar to a vision transformer (ViT) (See: [31]), the output image from the previous stage will be fed into a convoluted embedded patch layer so that the image features will be flattened, as shown in Figure 11, meanwhile, a learnable feature token will be appended to the newly flattened features, as shown in the left of Figure 12. Mathematically, this block with the output shown in Figure 11 can be represented as

$$\begin{aligned}
z_0 &= [x_{token}^0; x_{patch}^1 E; x_{patch}^2 E; \dots; x_{patch}^N E] + E_{position} \\
z'_i &= MSA(LN(z_{i-1})) + z_{i-1} \\
z_i &= MLP(LN(z'_i)) + z'_i \\
y_{image} &= Linear(Conv(z_i^{1:N})) \\
y_{token} &= Linear(LN(z_i^0))
\end{aligned}$$

where x_{patch}^i is the patches, N is number of patches, which can be calculated as $\frac{H \times W}{(\text{patch size}(P))^2}$ E s are the linear projection of flattened patches, a fully connected layer, which will map

the learned features onto sample space (See: [43]), E_{pos} is the positional encoder, MSA is the multi-head self-attention layer, LN is the linear normalization layer, MLP is the multi-layer perception layer, $linear$ is the fully connected linear layer, and $conv$ is the convolutional layer. For instance, for an image in the output of ResNet, $x_i \in \mathbb{R}^{1 \times 10 \times 10}$, with the patch size

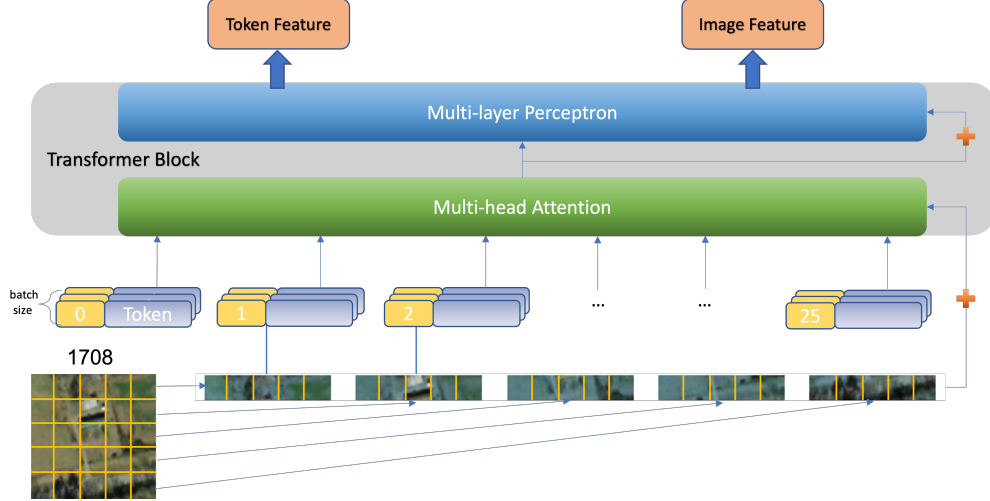


Figure 11: Vision Transformer

of 2, the flattened vector should have $\frac{H \times W}{P^2} = \frac{100}{4} = 25$ patches concatenate an additional token vector and positional encoding. The output dimension will become a $x \in \mathbb{R}^{(25+1) \times 4}$ features. Our model applied a convolution method to the image since our patch size is small, only 4, with the output channel 64. Thus, the output dimension of the embedded patch layer is $(26, 64)$.

Then, the data will have two transformer blocks, each of which will have a multi-head attention layer and a multilayer perception, as shown in the right of Figure 12. In the multi-head attention layer, the flattened input feature vectors with appending tokens will apply linear projections by multiplying three different weight, $w_i \in \mathbb{R}^{P^2C \times \frac{P^2C}{n_head}}$, $i \in \{q, k, v\}$ to three new vectors $Q(query)$, $K(key)$, and $V(value)$, for instance $w_q x = Q$. Thus, in this case, Query, key, and value vectors should have shape $(b, 26, 8, 8)$ as the hidden dimension is $64(8 \times 8)$. The n_head stands for the number of heads defined for multi-head attention. Vaswani et al.[30]. define the output of the attention layer as concatenating the various heads and then multiplying by a matrix w^o .

$$\text{concat}(head_1, \dots, head_h)w^o = head_1w_1^o + \dots + head_hw_h^o$$

where $w^o = \begin{bmatrix} w_1^o \\ \vdots \\ w_h^o \end{bmatrix}$ As the results are concatenated, the dimension is $\frac{P^2C}{n_head} \times n_head = P^2C$.

Thus, at the end of this layer, the dimension is still $\mathbb{R}^{P^2C \times P^2C}$. Once Q, K, V are obtained, the score could be computed by $\text{softmax}(QK^T)$, and logit are scaled by $\frac{1}{\sqrt{d_{qkv}}}$ for the scaled

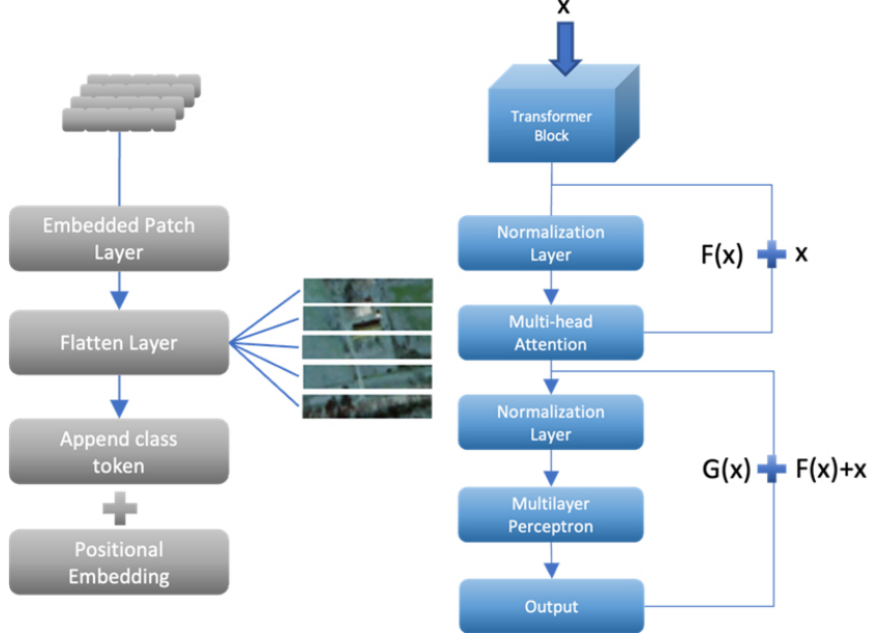


Figure 12: LEFT: Embedded Patch Layer; RIGHT: Transformer Block

dot-product score as follows,

$$Z = \text{softmax}\left(\frac{QK^T}{\sqrt{d_{qkv}}}\right)V,$$

where Z is scaled dot-product attention[30].

During multi-layer perception stage, the input will flow into a full connected linear layer with activation function Gaussian Error Linear Units(GELUs)[46] which is defined as

$$\begin{aligned} \text{GELU}(x) &= xP(X \leq x) \\ &= x \cdot \frac{1}{2}\left[1 + \text{erf}\left(\frac{x}{\sqrt{x}}\right)\right] \end{aligned}$$

and a dropout layer to prevent overfitting. In the last, linear layer the output dimension will be changed back to its origin. Thus the dimension of the vectors has no changes.

Instead of outputting a token class only like ViT, our model will also output image features, which can be treated as summarized features of an image. Thus, at the output stage of the wildfire image information network, we will have extra features for appending to the neural network model.

3.4. Hybrid Multimodal Model

In the hybrid model, the imagery data will be processed by the previous model and image features and token features will be the outputs from the process. Then the outputs will concatenate with the information data and fed the new concatenated data into the baseline model. Thus, as shown from Figure 13, the hybrid model will take the results from

Parameters	Values
Number of Layers	2
Patch Size	2
Number of Head	8
Multi-Layer Perceptron Neurons	8
Dropout Rate	0.2

Table 4: Hyperparameters for Transformer

wildfire images information net, then together with the information data into the baseline model. At the last stage, the output of the model will be the required target probabilities. In the metrics, the threshold is 0.5, which means if the probability is larger than 0.5, then the model is categorized as true or false. Mathematically, we can write

$$\hat{R} = \begin{cases} True, & \text{if } p > 0.5 \\ False, & \text{if } p \leq 0.5 \end{cases}$$

where \hat{R} are the responses, p is the outputs from the model. During the training, it usually reaches the top TPR and TNR at about 100 epochs. In the hybrid model, the model totally has 268615 variables.

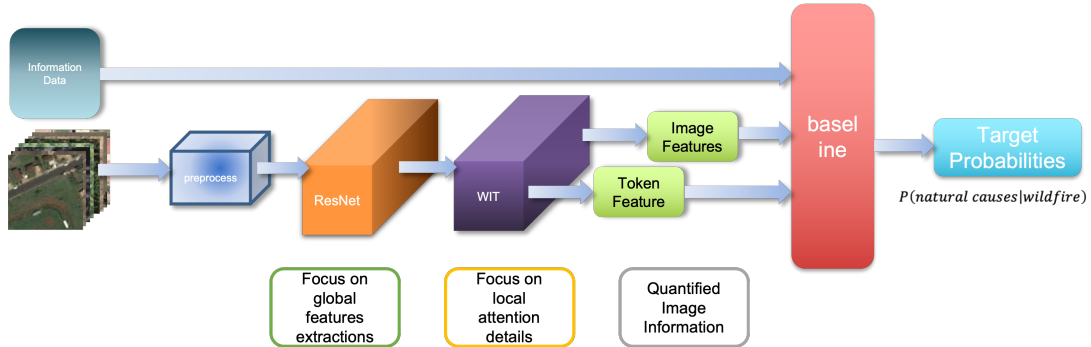


Figure 13: Hybrid Model Outline

4. Results and Discussions

4.1. Forecast Metrics

The metric used to measure the performance is the True Positive Rate (TPR or sensitivity) and true negative rate (TNR or selectivity) [47], which both are the components of accuracy. True positive is defined as values that are positive and predicted positive. In this case, the True Positive value indicates a scenario in which a wildfire that occurred in a given location was caused by natural causes, and the prediction also indicates that the wildfire is caused by natural causes. Thus, this value should be as large as possible. On the

contrary, a False Negative value represents a scenario in which a wildfire occurred in a given location, and the model predicts that it is due to natural causes, while they are not. This is a type II error; thus, it should be avoided. Therefore, a true positive rate with these two values can provide us with good performance metrics, Since the model tends to have a high true negative rate without using the undersampling method, finding optimal values between the true positive rate and the true negative rate is a top priority. It provides a conditional probability that if there is a wildfire, the model can categorize whether it is caused by nature or not.

The metric used to measure the performance is the True Positive Rate (TPR or sensitivity) and True Negative Rate (TNR or selectivity) [47], which both are the components of accuracy. True positive is defined as values that are positive and predicted positive. In this case, the True Positive value indicates a scenario in which natural causes caused a wildfire in a given location, and the model’s prediction also indicates that natural causes caused the wildfire. Thus, this value should be as significant as possible. On the contrary, a False Negative value represents a scenario in which a wildfire occurred in a given location, and the model predicts that it is due to natural causes, while they are not. This is a type II error; thus, it should be avoided. Therefore, a True Positive Rate with these two values can give us good performance metrics. Since the model tends to have a high true negative rate without the undersampling method, finding optimal values between the True Positive Rate and the True Negative Rate is a top priority. It provides a conditional probability that if there is a wildfire, the model can categorize whether it is caused by nature. Mathematically, we have

$$TPR = \frac{\textit{True Positives}}{\textit{True Positive} + \textit{False Negatives}} \quad (5)$$

$$TNR = \frac{\textit{True Negatives}}{\textit{True Negatives} + \textit{False Positives}} \quad (6)$$

There are other metrics often used in the analysis, F-score [48], which can be represented as

$$F\text{-score} = \frac{\textit{True Positives}}{\textit{True Positives} + 0.5(\textit{False Positive} + \textit{False Negative})}$$

and the precision or the positive predictive value, i.e.

$$\textit{Precision} = \frac{TP}{TP + FP} .$$

However, F-score and precision are not included here because, in our test case, the false counts are much more than the true ones, as shown in the equation. The F-score gives equal importance to precision and recall [49].

The precision is related to the proportion of true cases and false cases [50], (See Appendix 5). In our case, since precision will lead to some waste of resources, our top priorities are still *TPR* and *TNR*.

Using the terminology coined in this paper, as can be seen from Eq. (5), a high “True Positive” rate means that when the model predicts a fire in a certain area, there is actually a fire occurs, while the false negative indicates a low rate of “True Positive”, which means the possibility of misclassifying the real occurred wildfire.

The term “False Positive” in our terminology, means that there is no fire, and the model correctly categorizes it as no fire occurrence. If this rate is low, it indicates that there will be some false alerts as shown in Eq. (6), which may waste resources while ignoring the alert might be detrimental. Thus, currently, our focus will be first to increase the TPR , the TNR and hence the accuracy in reliability.

4.2. Baseline Model Results

The baseline model with recommended setting (See: 5) provides relatively stable results for all the baseline cases we trained. As we can see from Figure 14 (a), Figure 15 (a), and Figure 16 (a), 5 pre-trained results are chosen, which are also available in Colab. The variance of the losses of each case is relatively low for 5 random runs. However, with different selected features, the results are slightly improved.

As one can see from Figure 14 (a), the losses are successfully converged to a small but little higher value than 0.06. On the accuracy side, as shown in Figure 14 (b), the test accuracy at the last epoch 300 is all within the range of 89% to 90%.

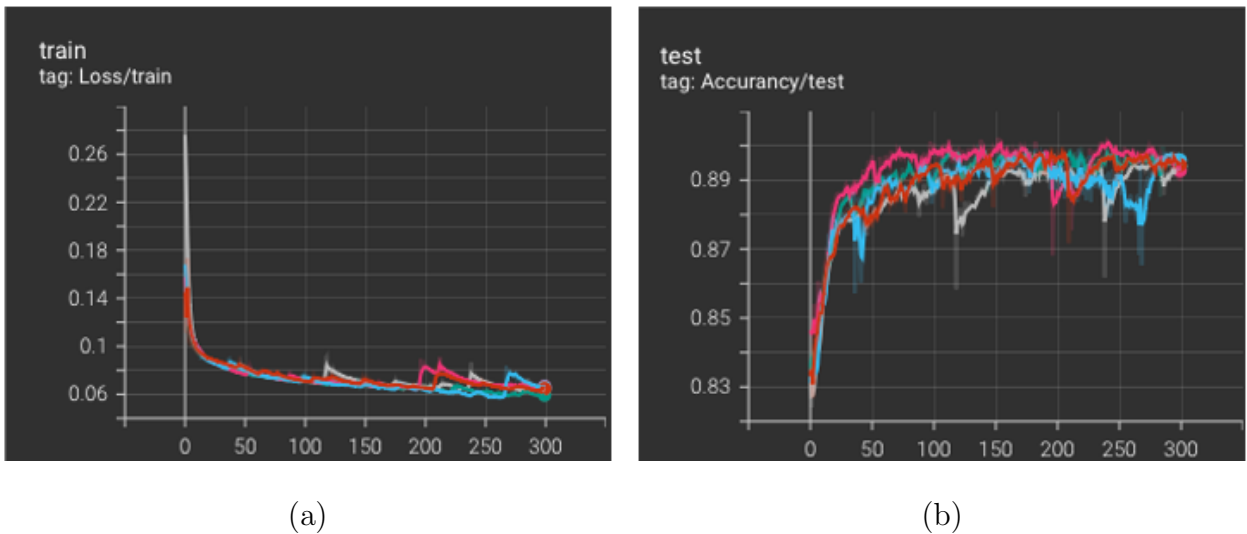


Figure 14: (a) Loss for data without vegetation category, and (b) Accuracy for data without vegetation category.

If we add vegetation categories as new features to the training dataset, with the same architecture as the hyperparameters, the results will be slightly improved as shown in Figure 15 (a). Compared with the previous one, the loss is slightly smaller, mostly within 0.06, as shown in Figure 17, the line in red is the result of not including the vegetation category, and the line in orange is the one with the vegetation category. The same situation occurs in test accuracy as shown in Figure 15 (b), we can see that the overall accuracy is better and some

of the results are more than 90% accuracy. Model Stability is one of the core principles in data science [51]. For each of the models, we randomly split train and test data, as shown in all errors, the baseline model is relatively stable. We can also see from Figure 17 (b) that the accuracy is even better if the features include the vegetation categories.

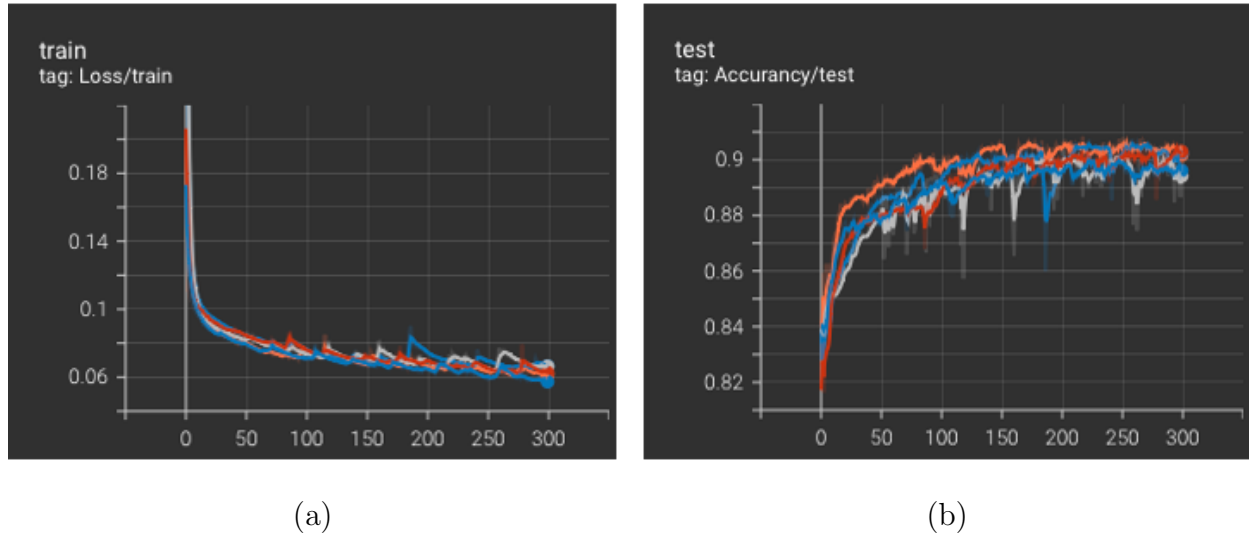
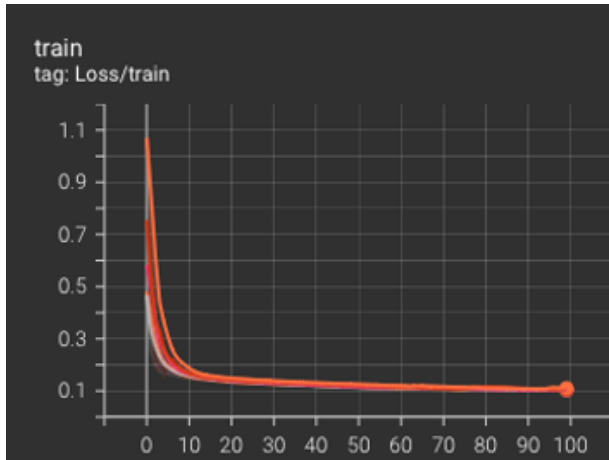


Figure 15: (a) Loss for data with vegetation category, and (b) Accuracy for data with vegetation category.

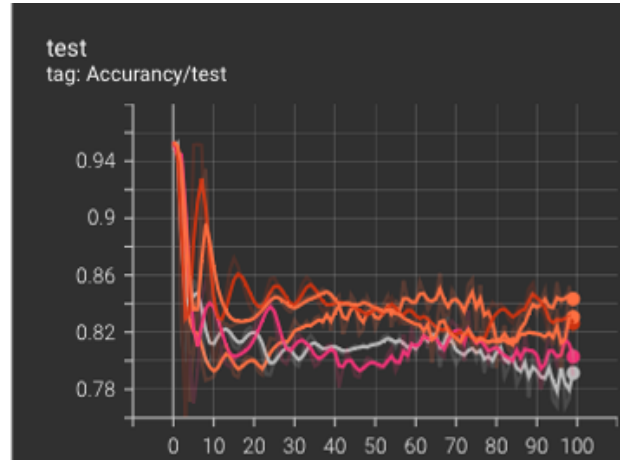
As we can see from Figure 16 (a) if we use the undersampling data for training, the losses are higher than previous case, and the accuracies are also lower, which is around 82%. The reason for the high accuracy is due to the imbalance of data. The model tends to categorize as false since more than 80% data are false. Thus, the model fits well for categorizing most cases as false.

As shown in Figure 18 (a), we can see that among 5910 test data, 5015 are categorized as negative, which leads to a 94.6% TNR. Even though it is a little better with vegetation categories, a similar situation occurs in the cases with vegetation category, as shown in Figure 18 (b), among the same amount of test data, 5910 and 4985 are categorized as false. For sensitivity, the results are similar to those without the vegetation category, which is also more than 90%. For specificity, compared to the previous one, we can see that the results are about 5% better. Even with limited improvement, these results are better than the previous. Thus, specificity contributed the most accurately since it has a large proportion and relatively high results. As we mentioned, sensitivity is the top priority and the part that we care about most, by using these features, the sensitivity is not high enough even though it provides a high accuracy. Thus, if we only used 7 days, 15 days, and 30 days' average temperature and wind data as features, the neural network model converges but with around 89% accuracy and quite low sensitivities (65% – 70%) with a high specificity with more than 90%, as shown in Figure 18 (a).

After applying the undersampling method, we can see the results from Figure 18 (c), even though the weighted accuracy is lower than in previous cases, the *TPR* increases a lot to more than 80%. For a total of 18985 test cases, the model found an optimal solution

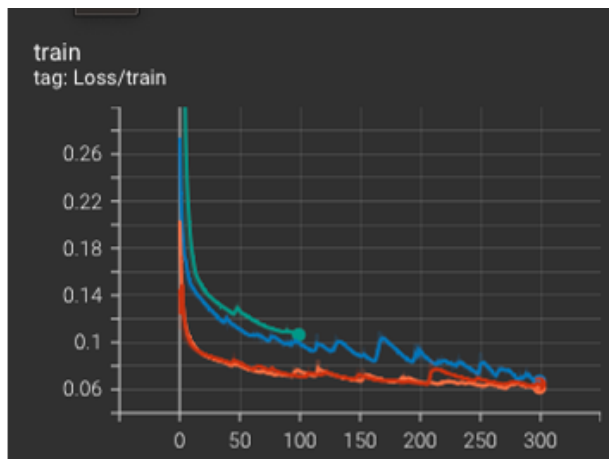


(b)

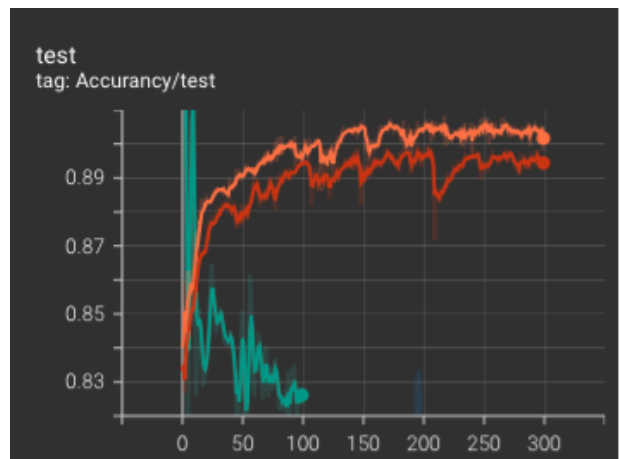


(b)

Figure 16: (a) Loss for undersampling data with vegetation category, and (b) Accuracy for undersampling data with vegetation category



(a)



(b)

Figure 17: (a) Comparison of losses, and (b) Comparison of accuracy

to balance the TPR and TNR , which are around 80%, leading to the total accuracy also about 80%. This is the desired result.

Then if we add 7 days, 15 days, and 30 days of average humidity or precipitation data, the neural network model converges, and losses are around 0.07 and accuracy is around 88% – 89%, the confusion matrix is not good since the sensitivities are less than 60%. Once we added vegetation-type data, the losses decreased by about 0.01 to 0.05 – 0.06 and accuracy will increase around 1%, the sensitivity of confusion matrix increases to around more 60% – 65%.

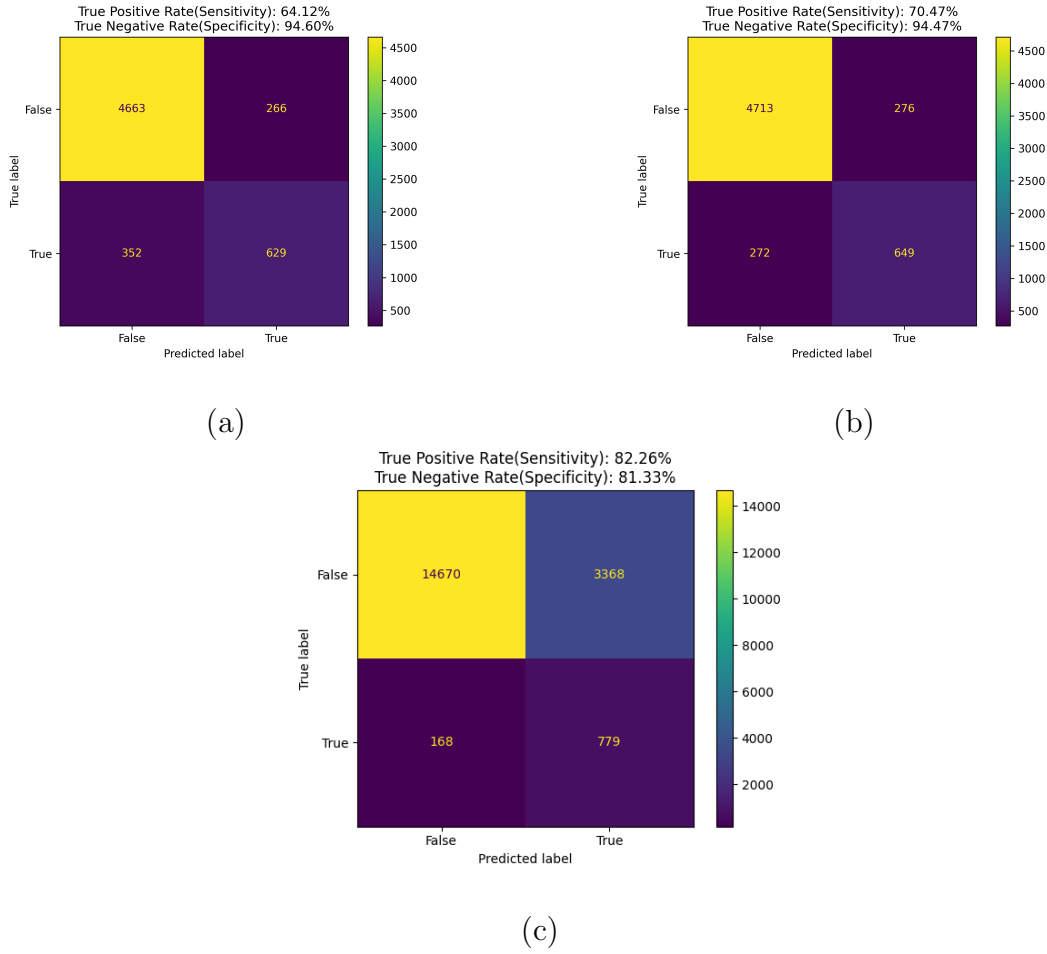


Figure 18: (a) Confusion matrix for data without vegetation category, (b) Confusion matrix for data with vegetation category, and (c) Confusion matrix for undersampling model.

4.3. Hybrid model results

Figure 19 shows how some images change during different stages from a pre-trained model, we can see the top of Figure 19 is the original grey-scale image and the output of the first convolutional layer of the same index are the middle images. After the first trained convolutional layer, the trained results successfully maintain the features from the original images. We are able to see the obvious features from the previous original images. For the bottom of Figure 19, due to the resolution being quite small, which is 10×10 , we can see some similarities if compared with the original images. Thus, when finishing training, the convolutional part extracts feature maps from the images and feeds them to the next stage.

Figure 20 is the output of the pre-trained model with the same index from Figure 19. The original images have a resolution of 5×5 , even with a small resolution, we believe that this is how the model sees the images and finds the features of a certain condition for the model. Figure 5 shows detailed outputs for each layer.

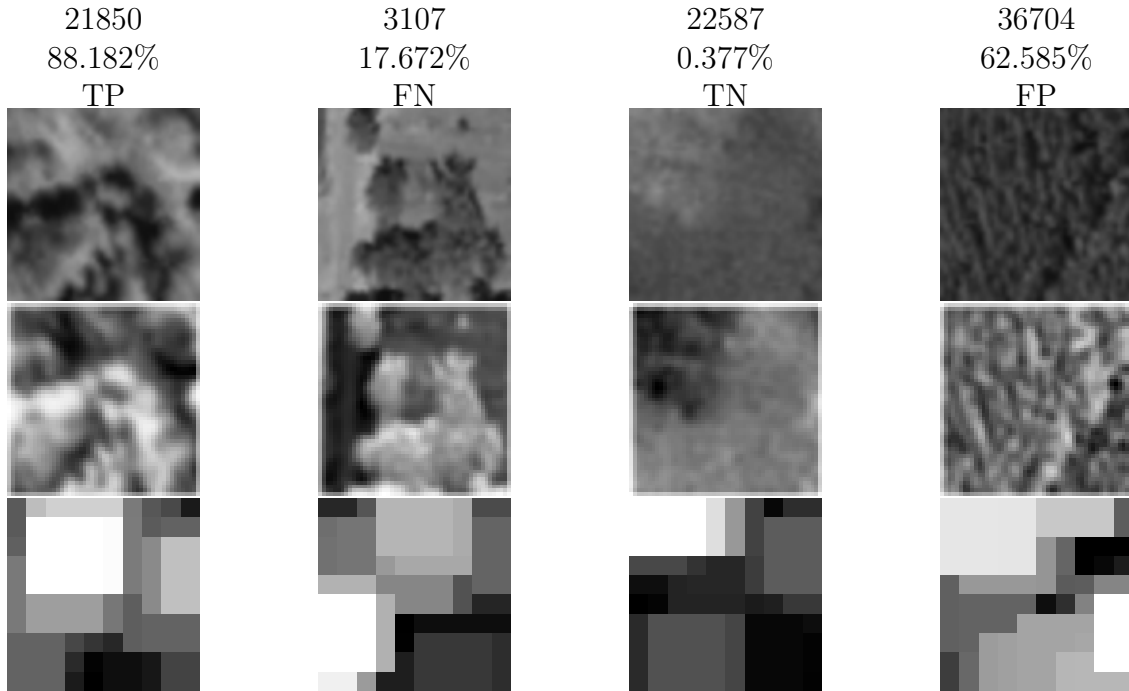


Figure 19: Sample outputs of ResNet with their predicted probabilities and confusion matrix categories. TOP: original gray-scaled images ($H : 100 \times W : 100$); MIDDLE: outputs of first convolutional layer (first principle component) ($H : 51 \times W : 51$); BOTTOM: outputs of last layer ($H : 10 \times W : 10$)

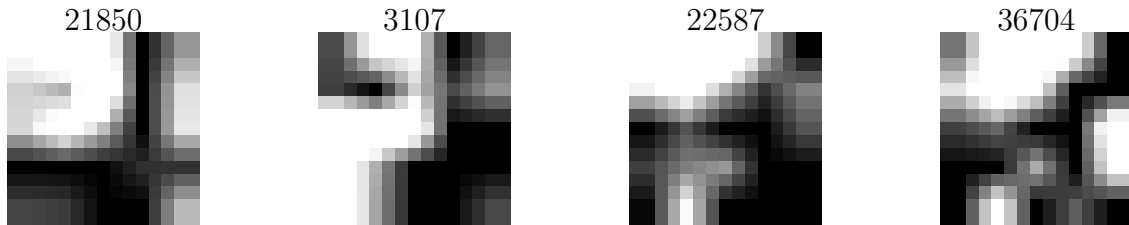
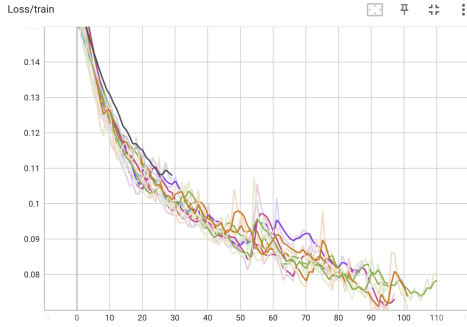


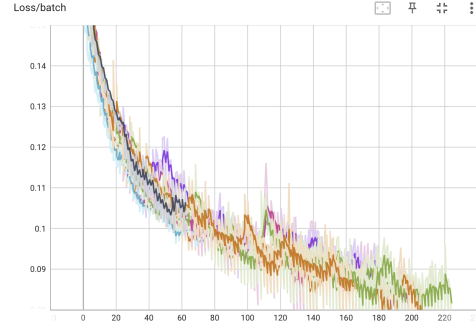
Figure 20: Sample outputs of Transformer stage. Images are up-sampled by scale factor 3 ($H : 15 \times W : 15$) with bilinear mode

As we can see from Figure 21, the loss successfully converged and reached in a range of 0.07 to 0.08. Our top priority, TPR reaches 85% while the TNR also reached 85% during that within that range of losses. Therefore, our accuracy is also around 85% as calculated by $\frac{TPR+TNR}{P+N}$, as shown in Figure 22. However, we can see from both of the confusion matrices in Figure 18 (c) and Figure 22, the precisions are relatively low since inside the test case for undersampling, we move some majorities to the test case. This is one of the drawbacks of this model. If we have a low precision, it means that there is a high probability that there would not be a fire, but we categorized it as true, which causes a false alarm, and a type II error will occur.

Usually, based on the experiences, during training, about 60 epoch, the TPR and TNR will both reach around 80% and so does accuracy. When reaching 100 epochs, all of them might be more than 83%.

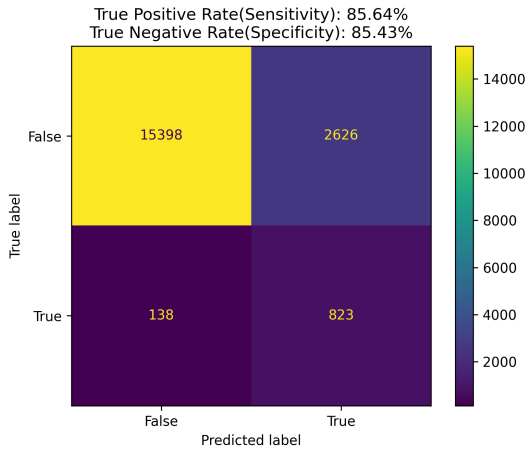


(a)

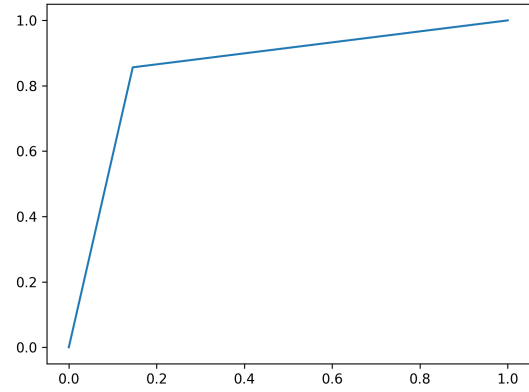


(b)

Figure 21: (a) Epoch losses (left) and (b) scaled batch losses (right) of hybrid model



(a)



(b)

Figure 22: (a) Confusion matrix (left) and (b) ROC curve (right) for hybrid model results

4.4. Main results

From Table 5, we summarized the results of our experiments. As shown, the best TNR is in all the features without images and undersampling method. Even though with a TPR about 70%, the precision is relatively high, which means that the model can predict accurately within the true cases. However, there is a trade-off, with the TPR increase, our TNR experiment results go down 10%, as shown in Table 5. So does the precision, since the precision is related to the proportion of our data as shown in Appendix 5, among the 18955 test cases, there are only 5% with the true label, even 85% of them are categorized right, the precision, $\mathbb{P}(actual = True | predict = True)$, went down to about 23.86% from Figure 22, with a 5% increase from the results, 18.78%, of the features without images.

As we can see from Figure 23 (b), another optimal case, the results without adding the majority to the test case, we still have about 85% accuracy. Since all true cases are in the original test cases the TPR will not change. We can see that from both Figures 23 (a) and

Model	Features Used	loss	Top Accuracy(%)	Top TPR(%)	Top TNR(%)
Baseline	t,w	≥ 0.12	≤ 85	40 ~ 50	≈ 82
	t,w,h,p	≥ 0.06	88 ~ 89	63 ~ 68	92 ~ 95
	t,w,h,p,v	≈ 0.06	89 ~ 90	65 ~ 70	≈ 95
	undersample all	≈ 0.06	≥ 80	75 ~ 82	80 ~ 81
Hybrid	undersample image	≤ 0.1	≈ 85	≈ 85	≈ 85

Table 5: top 5% of metrics, note:t=temperature, w=wind, h=humidity, p=precipitation, v=vegetation, all=all features

23 (b), for the added majorities, which has 16343 cases with all false, the TN is about 13885 and FP is 2458, Thus, the TNR is about 84.96% which is also the accuracy in this case since there are no true results in this part. However, if we do not include the majority of test cases, the precision can reach about $\frac{787}{245+787} = 76.26\%$, since our overall accuracy is still about 85%, with more false cases, the precision will go down. Therefore, the proportion of the data will have a large influence on the precision. If we include more true data later, the precision should go up. Moreover, once both TPR and TNR are improved, the precision should also be improved.

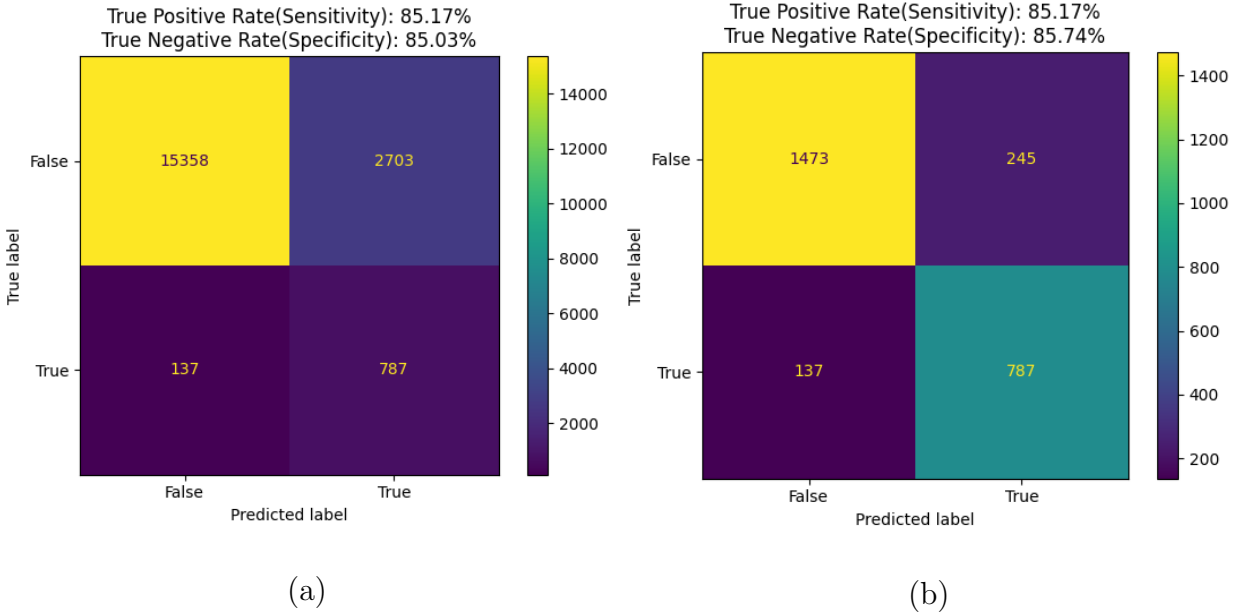


Figure 23: (a) Confusion matrix with full test, and (b) Confusion matrix without majorities.

4.5. Case Study: 2018 California Camp Fire

To demonstrate and validate the ability and effectiveness of the proposed high-resolution multimodal transformer neural network model to forecast or predict wildfire occurrence, we used the local weather forecasting data on November 7th, 2018, and the local Google Earth

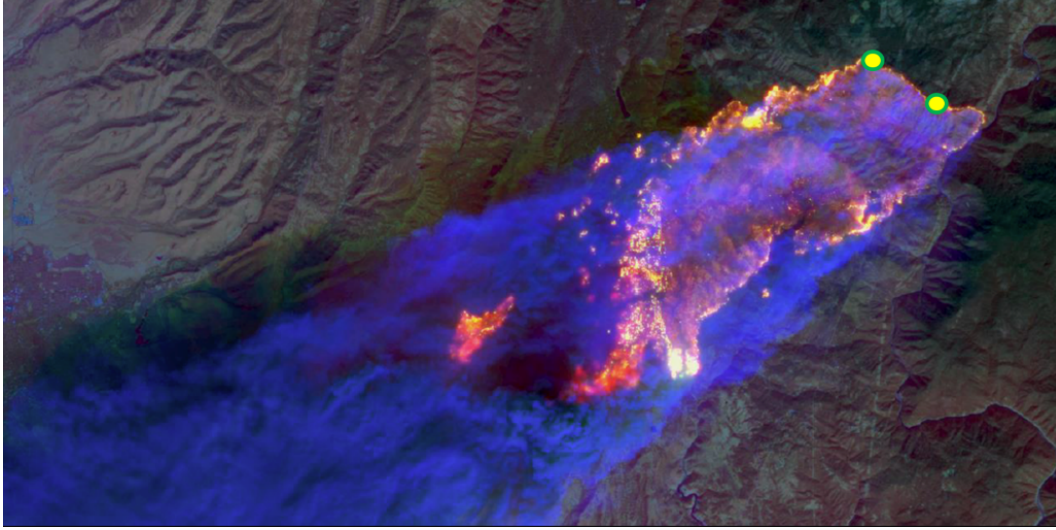


Figure 24: Landsat 8 overpass of the Camp Fire on November 8, 2018, at 1:44 pm EST (10:44 am PST). Credits:NASA/Marshall Space Flight Center/United States Geological Survey [52])

image data before November 7th, 2018, in the vicinity of Pulga, California, just right before the occurrence of the 2018 California Camp (November 8th, 2018) to test the performance of the proposed Bayesian machine learning model.

Figure 24 is a real satellite image taken right after the starting occurrence of the California Camp Fire near the town of Pugla, California, on November 8th, 2018, by NASA.

The two fire starting or occurrence locations are marked as colored circles (I: Orange circle and II: Red circle.) in Figure 24.

By inputting the local weather data and the image data from Google Earth into the multimodal transform neural network, the multimodal transformer machine learning neural network will output the probability distribution in the local region. Figure 25 is the prediction result obtained by using the proposed multimodal transformer neural network model on prediction of the occurrence of the California Camp Fire at the observed fire occurrence site I. The topographic and weather information input data and parameters are given as follows,

[39.831119, -121.480039, 18.74354839, 18.240000, 18.30714286,
16.20967742, 16.680000, 16.57142857, 37.60000, 39.93333333,
34.61428571, 0.0000, 0.0000, 0.0000]

where the first two are the converted longitude and latitude of the location. The next 12 parameters are the average temperature, wind speed, and precipitation, humidity for the prior 7, 15, and 30 days before November 8th, 2018. The last 6 are the vegetation categories for this location. This row is repeated 195 times since this area shares the same data value, the only difference is the 195 different input images as shown in Figure 25.

The predicted wildfire probabilities on each small-scale box of $100m \times 100m$ are depicted in Figure 25. We marked all the wildfire occurrences with high probability ($> 70\%$) regions with yellow color probability numbers.



Figure 25: Prediction results for the 2018 California Camp Fire occurrence location I.

For the fire occurrence location II, we also input the local geographic and weather data, as well as Google Earth image data into the Bayesian machine learning neural network. The input information data is given as follows,

[39.825097,-121.446211, 18.74354839, 18.240000, 18.30714286,
 16.20967742, 16.680000, 16.57142857, 37.60000, 39.93333333,
 34.61428571, 0.0000, 0.0000, 0.0000]

The predicted wildfire probabilities on each small-scale box of $100m \times 100m$ are depicted in Figure 26. Again, we marked all the wildfire occurrences with high probability ($> 70\%$) regions with yellow color probability numbers as shown in Figure 26.

It is worth noting that the training data that we used is from 1992 to 2015, while the California Camp Fire occurred in 2018. Therefore, this example is a bona fide forecasting demonstration.

From Figures 25 and 26, One may find that the places where wildfires most likely occur are regions with dense vegetation and flat terrain.

5. Conclusions and Perspectives

In this work, we developed a high-resolution multimodal transformer neural network model to forecast wildfire hazard occurrence location and timing at a small scale. Different from the existing ML models for wildfire prediction, the present approach combines weather information, historical fire data, local topographic information, and Google Earth image information to train the multimodal transformer neural network machine learning model, and then practically provides the wildfire occurrence forecast at a local spatial location within



Figure 26: Prediction results for the 2018 California Camp Fire occurrence location II.

$\leq 100m^2$. By using the wildfire data in the United States from 1992 to 2015 (USDA[9]) to train the high-resolution multimodal transformer neural network, we can provide the small-scale spatial probability of wildfire occurrence with the input of the given weather forecasting information and the synchronized local Google Earth imagery information 24 hours before. This is a significant advance in wildfire forecasting and prediction technology, and we have made a major step forward in wildfire occurrence forecasting.

Moreover, in this work, we use the wildfire data collected in the *FPA_FOD* database to demonstrate the viability and the accuracy of the proposed artificial intelligence-based wildfire forecast system. The fourth edition of *FPA_FOD* ([7]) contains 1.88 million entries of wildfire records from 1992 to 2015. Recently, a new version with 2.3 million entries of wildfire records was released to the public [53]. It contains a spatial database of wildfires that occurred in the US from 1992 to 2022, which is the 7th edition of the wildfire database to support the National Fire Program Analysis (FPA) system[53].

Thus, based on this new database, we can use a database with more data information, and more data features, and better-quality data to train the proposed Bayesian machine learning neural network. The new database version increases about 42 thousand wildfire records within 5 years. As mentioned before, some of the images from Google Earth are in grayscale before 2005, however, with this newly released data, we should be able to use the colored images of vegetation and extract terrain topological features.

Moreover, all the occurrences from *FPA_FOD* are within the US, and recently, a data called Wildfire Prediction Dataset (Satellite Images) was also released[54]. It is based on wildfire data from Canada’s Open Government Portal[55]. It contains two categories: wildfire images and no wildfire images. We can use wildfire images to increase and enrich the data set. Furthermore, we may even be able to add more data, such as Global Fire Emis-

sions Database version 4[56]. Combining with and extending remote sensing data[57] that was collected from MODIS (Moderate Resolution Imaging Spectroradiometer). Besides the data collected from North America.

Moreover, all the occurrences from *FPA_FOD* are within the US, and recently, a data called Wildfire Prediction Dataset (Satellite Images) was also released[54]. It is based on wildfire data from Canada’s Open Government Portal[55]. It contains two categories: wildfire images and no wildfire images. We can use wildfire images to increase and enrich the data set. Furthermore, we may even be able to add more data, such as Global Fire Emissions Database version 4[56]. Combining with and extending remote sensing data[57] that was collected from MODIS (Moderate Resolution Imaging Spectroradiometer).

Besides the data collected from North America. the wildfire data in other parts of the world may also be available [58]. With more data, not only the neural network model could perform better, but the transformer like the model, will also have a better performance since, as we mentioned before, a transformer usually requires a large amount of data[41]. As mentioned in 2.4, the accuracy of the data may significantly affect the prediction outcome. Therefore, for a certain location, if the data quality could be better, especially for the image data, the accuracy could significantly be increased. In the present work, some of the features that are still missing from the database, such as elevation or sensing data. Remote sensing data can also be added to the data if the amount data collected is enough, which can also help predict wildfire occurrence[59]. We shall report an updated version of the multimodal transformer neural network model for wildfire prediction in subsequent work.

References

References

- [1] V. Samborska, H. Ritchie, and M. Roser. Wildfires. Our World in Data, 2024. <https://ourworldindata.org/wildfires>.
- [2] A. Bolt, C. Huston, P. Kuhnert, J.J. Dabrowski, J. Hilton, and C. Sanderson. A spatio-temporal neural network forecasting approach for emulation of firefront models. In IEEE 2022 Signal Processing: Algorithms, Architectures, Arrangements, and Applications (SPA), pages 110–115, September 2022.
- [3] J.J. Dabrowski, D.E. Pagendam, J. Hilton, C. Sanderson, D. MacKinlay, C. Huston, A. Bolt, and P. Kuhnert. Bayesian physics informed neural networks for data assimilation and spatio-temporal modelling of wildfires. Spatial Statistics, 55:100746, 2023.
- [4] Cavard Xavier, Boucher Jean-François, and Bergeron Yves. Vegetation and topography interact with weather to drive the spatial distribution of wildfires in the eastern boreal forest of canada. International Journal of Wildland Fire, 24:391–406, 2015.
- [5] Kostas Kalabokidis, Alan Ager, Mark Finney, Athanasios Nikos, Palaiologos Palaiologou, and Christos Vasilakos. Aegis: A wildfire prevention and management information system. Natural Hazards and Earth System Sciences, 16:643–661, 03 2016.
- [6] Brean W. Duncan, Frederic W. Adrian, and Eric D. Stolen. Isolating the lightning ignition regime from a contemporary background fire regime in east-central florida, usa. Canadian Journal of Forest Research, 40(2):286–297, 2010.

- [7] Matt P. Plucinski. A review of wildfire occurrence research, 2021.
- [8] A.H. Taylor, H.M. Poulos, J. Kluber, and et al. Controls on spatial patterns of wildfire severity and early post-fire vegetation development in an arizona sky island, usa. Landscape Ecol, 36:2637–2656, 2021.
- [9] Karen C. Short. Spatial wildfire occurrence data for the united states, 1992-2015(4th edition), 10 2017.
- [10] David Harris and Sarah Harris. Digital design and computer architecture. Morgan Kaufmann, San Francisco, California, 2012.
- [11] Google. Google earth pro, 2023.
- [12] National Centers for Environmental Information. National centers for environmental information, 2023.
- [13] OPeNDAP software. Opendap, 11 2023.
- [14] Varun. Wildfire data analysis, 10 2020.
- [15] Landsat Science. Landsat science, 2023.
- [16] Sentinel Online. Sentinel online, 2023.
- [17] Rodolfo Urbano Batista. Pullover’s marco creator, 11 2021.
- [18] Rafael C. González and Richard Eugene Woods. Digital Image Processing. Prentice Hall, 2007.
- [19] F.J Pérez-Invernón, F.J Gordillo-Vázquez, H Huntrieser, and et al. Variation of lightning-ignited wildfire patterns under climate change. International Journal of Wildland Fire, 14:739, 2023.
- [20] Sergi Costafreda-Aumedes, Carles Comas, and Cristina Vega-García. Human-caused fire occurrence modelling in perspective: a review. International Journal of Wildland Fire, 26:983–998, 2017.
- [21] Coogan Sean C. P., Aftergood Olivia, and Flannigan Mike D. Human- and lightning-caused wildland fire ignition clusters in british columbia, canada. International Journal of Wildland Fire, 31:1043–1055, 2022.
- [22] Mengqi Yao, Meghana Bharadwaj, Zheng Zhang, Baihong Jin, and Duncan S Callaway. Predicting electricity infrastructure induced wildfire risk in california. Environmental Research Letters, 17(9):094035, 9 2022.
- [23] H. He, Y. Bai, E. A. Garcia, and S. Li. Adasyn: Adaptive synthetic sampling approach for imbalanced learning. In 2008 IEEE International Joint Conference on Neural Networks (IEEE World Congress on Computational Intelligence), pages 1322–1328, 2008.
- [24] N. V. Chawla, K. W. Bowyer, L. O. Hall, and W. P. Kegelmeyer. SMOTE: Synthetic minority over-sampling technique. Journal of Artificial Intelligence Research, 16:321–357, 6 2002.
- [25] Piyush Jain, Sean C.P. Coogan, Sriram Ganapathi Subramanian, Mark Crowley, Steve Taylor, and Mike D. Flannigan. A review of machine learning applications in wildfire science and management. Environmental Reviews, 28(4):478–505, 2020.
- [26] National Wildfire coordinating Group. Probability of ignition, August 2021.
- [27] JJ Hopfield. Neural networks and physical systems with emergent collective computational abilities. Proceedings of the National Academy of Sciences of the United States of America, 79(8):2554—2558, 4 1982.
- [28] Keiron O’Shea and Ryan Nash. An introduction to convolutional neural networks, 2015.
- [29] Kaiming He, Xiangyu Zhang, Shaoqing Ren, and Jian Sun. Deep residual learning for image recognition, 2015.
- [30] Ashish Vaswani, Noam Shazeer, Niki Parmar, Jakob Uszkoreit, Llion Jones, Aidan N. Gomez, Lukasz Kaiser, and Illia Polosukhin. Attention is all you need, 2017.
- [31] Alexey Dosovitskiy, Lucas Beyer, Alexander Kolesnikov, Dirk Weissenborn, Xiaohua Zhai, Thomas Unterthiner, Mostafa Dehghani, Matthias Minderer, Georg Heigold, Sylvain Gelly, Jakob Uszkoreit, and Neil Houlsby. An image is worth 16x16 words: Transformers for image recognition at scale, 2021.
- [32] Yann LeCun, Yoshua Bengio, and Geoffrey Hinton. Deep learning. Nature, 521:436–444, 2015.
- [33] Sergey Ioffe and Christian Szegedy. Batch normalization: Accelerating deep network training by reducing internal covariate shift. In Francis Bach and David Blei, editors, Proceedings of the 32nd International Conference on Machine Learning, volume 37 of Proceedings of Machine Learning Research, pages 448–456, Lille, France, 7 2015. PMLR.
- [34] Abien Fred Agarap. Deep learning using rectified linear units (relu), 2019.

- [35] Shibani Santurkar, Dimitris Tsipras, Andrew Ilyas, and Aleksander Madry. How does batch normalization help optimization?, 2019.
- [36] Zhilu Zhang and Mert Sabuncu. Generalized cross entropy loss for training deep neural networks with noisy labels. In S. Bengio, H. Wallach, H. Larochelle, K. Grauman, N. Cesa-Bianchi, and R. Garnett, editors, Advances in Neural Information Processing Systems, volume 31. Curran Associates, Inc., 2018.
- [37] Thomas M. Cover and Joy A. Thomas. Elements of Information Theory (Wiley Series in Telecommunications and Signal Processing). Wiley-Interscience, USA, 2006.
- [38] Ian J. Goodfellow, Yoshua Bengio, and Aaron Courville. Deep Learning. MIT Press, Cambridge, MA, USA, 2016. <http://www.deeplearningbook.org>.
- [39] Diederik P. Kingma and Jimmy Ba. Adam: A method for stochastic optimization, 2017.
- [40] Chris Perry. Colab’s ‘pay as you go’ offers more access to powerful nvidia compute for machine learning, 2022.
- [41] Ran Shao and Xiao-Jun Bi. Transformers meet small datasets. IEEE Access, 10:118454–118464, 2022.
- [42] Alec Radford, Karthik Narasimhan, Tim Salimans, and Ilya Sutskever. Improving language understanding by generative pre-training, 2018.
- [43] L. Alzubaidi, J. Zhang, A.J. Humaidi, and et al. Review of deep learning: concepts, cnn architectures, challenges, applications, future directions. Journal of Big Data, 8(53), 2021.
- [44] F Berzal. Redes neuronales and deep learning 1: Entrenamiento de redes neuronales artificiales. Editorial Independiente. Madrid, Md, España, 2019.
- [45] Shaoqing Ren, Kaiming He, Ross Girshick, Xiangyu Zhang, and Jian Sun. Object detection networks on convolutional feature maps, 2016.
- [46] Dan Hendrycks and Kevin Gimpel. Gaussian error linear units (gelus), 2020.
- [47] Tom Fawcett. An introduction to roc analysis. Pattern Recognition Letters, 27(8):861–874, 2006. ROC Analysis in Pattern Recognition.
- [48] Cyril Goutte and Eric Gaussier. A probabilistic interpretation of precision, recall and f-score, with implication for evaluation. In David E. Losada and Juan M. Fernández-Luna, editors, Advances in Information Retrieval, pages 345–359, Berlin, Heidelberg, 2005. Springer Berlin Heidelberg.
- [49] David Hand and Peter Christen. A note on using the f-measure for evaluating record linkage algorithms. Statistics and Computing, 28(3):539–547, 2017.
- [50] Jesse Davis and Mark Goadrich. The relationship between precision-recall and roc curves. In Proceedings of the 23rd International Conference on Machine Learning, ICML ’06, page 233–240, New York, NY, USA, 2006. Association for Computing Machinery.
- [51] Bin Yu and Karl Kumbier. Veridical data science. Proceedings of the National Academy of Sciences, 117(8):3920–3929, 2020.
- [52] Jessica Sheaves. Trial by fire: What brady helms learned from the 2018 camp fire, 2021. Online.
- [53] Karen C. Short. Spatial wildfire occurrence data for the united states, 1992-2020(6th edition), 10 2022.
- [54] Abdelghani Aaba. Wildfire data analysis, 2 2023.
- [55] Government of Canada. Forest fires, 2017.
- [56] Global fire emissions database, version 4, (gfedv4), 2018.
- [57] Younes Oulad Sayad, Hajar Mousannif, and Hassan Al Moatassime. Predictive modeling of wildfires: A new dataset and machine learning approach. Fire Safety Journal, 104:130–146, 2019.
- [58] Dario Rodriguez-Aseretto, Daniele de Rigo, Margherita Di Leo, Ana Cortés, and Jesús San-Miguel-Ayanz. A data-driven model for large wildfire behaviour prediction in europe. Procedia Computer Science, 18:1861–1870, 2013. 2013 International Conference on Computational Science.
- [59] Yongjia Song and Yuhang Wang. Global wildfire outlook forecast with neural networks. Remote Sensing, 12(14), 2020.
- [60] Adam Paszke, Sam Gross, Francisco Massa, Adam Lerer, James Bradbury, Gregory Chanan, Trevor Killeen, Zeming Lin, Natalia Gimelshein, Luca Antiga, Alban Desmaison, Andreas Kopf, Edward Yang, Zachary DeVito, Martin Raison, Alykhan Tejani, Sasank Chilamkurthy, Benoit Steiner, Lu Fang, Junjie Bai, and Soumith Chintala. Pytorch: An imperative style, high-performance deep learning library. In Advances in Neural Information Processing Systems 32, pages 8024–8035. Curran Associates, Inc.,

2019.

[61] National Wildfire coordinating Group. Wildfire cause standard summary, August 2020.

Supplementary Materials

1. README File

In this Supplementary material, we provide a README file for readers to assist anyone who wishes to run the related computer code of the high-resolution multimodal transformer neural network model described in this paper. The interested readers can write to the corresponding author of this paper requesting the source code of the computer program. The reader should be able to run this code either on your own machine or on Google Colab.

1. Local machine: If running on local machine, please run

```
$ pip install -r requirements
```

or during running it will automatically checking satisfaction for requirements

2. Online Colab: First cell will check the requirements. Colab is available here

1.1 Requirements

- Python 3.6+
- PyTorch 2.0.0+[60]

1.2 Usage

The script and data are available from

Data Name	Size
Scripts & Codes	47K
Information Data	6.29M
Imagery Data	1.10G
Original Image Captures	TBD
Pre-trained model	34.2M
FPA_FOD_20170508 Wildfire information	NA
NOAA weather information	NA

Table .6: Data URL

1.2.1 Run the code locally

Example command for run a combined model:

```
$ python train.py --with-vegetation=True\  
                  --satellite -img=True\  
                  --gray-scale=True\  
                  --resample-method='undersampling'\  
                  --archive=True\  
                  --
```

```

—model-selection='hybrid-model'\
—learning-rate=0.01\
—epochs=100\
—display_step=10\
—batch=True\
—batch-size=64

```

This command in terminal will allow training the model vegetation and image features using undersampling method. The model is hybrid model with 64 mini-batches. It will run 100 epochs with learning rate 0.01, for every 10 steps, and then it will display the loss or accuracy. After finishing training, the model will be saved to './saved_progress'.

You can also run it with

```
$ python train.py -h
```

to see help and all available arguments.

Or using UI as following by running

```
$ python wildfire_ui.py
```

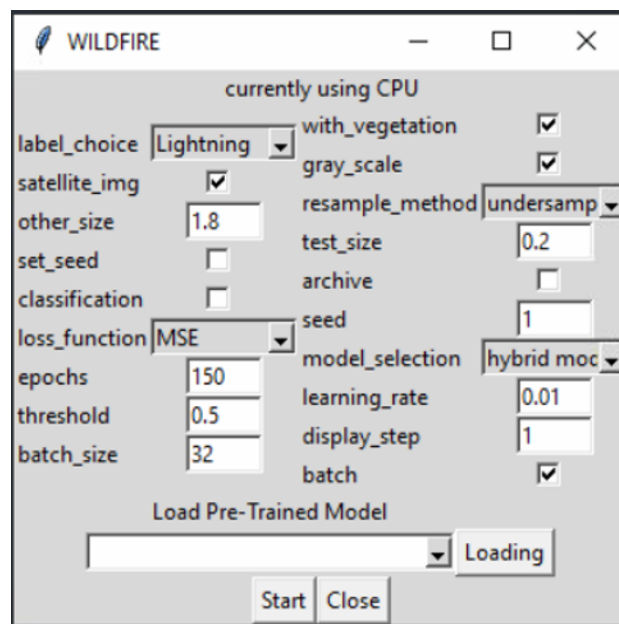


Figure .27: User Interface

This UI will not run the program, instead it will generate a command state in 5.

1.2.2 Instructions on Colab

First time run steps:

1. Loading Required Package
2. Create Symbolic Link

3. Util Functions
4. Parameter Setting
5. Read Subset Data & Create DataFrame
6. Create Dataset (Train set & Test set)
7. Neural Network (or F-CNN & ResNet)*
8. Hybrid Model
9. Initialize model
10. Training

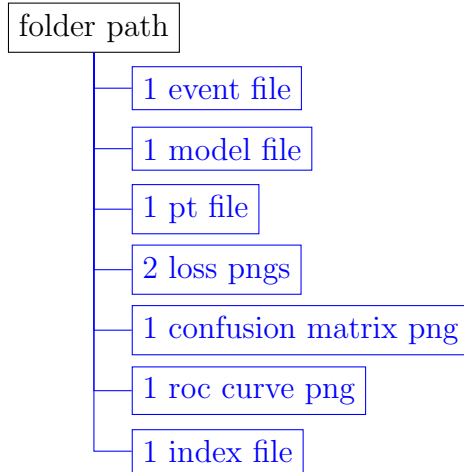
- Repeat training:
 - Training (step 10)
- Re-train a new model with same data
 - Initialize model (step 9)
 - Training (step 10)
- Train a new model with new shuffle data
 - Create Dataset (Train set & Test set) (step 6)
 - Initialize model (step 9)
 - Training (step 10)
- Train a new model with some arguments change
 - Parameter Setting (step 4)
 - Read Subset Data & Create DataFrame (step 5)**
 - Create Dataset (Train set & Test set) (step 6)**
 - Initialize model (step 9)
 - Training (step 10)
- Results
 1. Accuracy
 2. Confusion matrix
 3. Tensorboard
- Load pre-trained model***

```
import torch
model = torch.load(<desired model path>)
```

Here the symbol * indicates it applying to any desired models

The symbol ** indicates it applying when change input data (i.e test size, undersampling)

The symbol *** indicates that the saved progress may include 8 files



Event file stores the log information for training and test, model and .pt files store the model and all parameters separately, loss PNGs are the plots for the loss based on epochs or batch steps, confusion matrix png file displays the confusion matrix as a table, roc curve png show the ROC curve for the confusion matrix, and index file contains the random indices when data was shuffled and split for training and test initially for reuse purpose.

Params	Baseline	Hybrid
w/ veg	True	True
udersample	≥ 1.5	≥ 1.5
test size	≥ 0.15	≥ 0.15
learning rate	0.01	0.01
epochs	≤ 300	≤ 50

Table .7: Recommended Tuning

1.3 Parameter Descriptions

Parameters	Descriptions	Type
connect to google drive	allowing script connect to user's Google Drive	boolean
download_pre_trained	download pre-trained model	boolean
label choice	choose desired label	string
with vegetation	check box for vegetation categories as features	boolean
satellite images	check box for satellite images as features	boolean
resample method	choose resample methods	string
other size	with previous checked, choosing proportion for undersampling	float
test size	the proportion of test set	float
archive	check box for save the results	boolean
set seed	check box for control the randomness	boolean
seed	the seed for randomness	integer
model selection	select training models	string
loss function	choose loss function	string
learning rate	learning rate for optimizer	float
epochs	the amount of iterations training will run	integer
display steps	show the loss and accuracy	integer
threshold	a number larger than it will be false otherwise true	float
batch	check box for allowing batch during training	boolean
batch size	with previous checked, the size of each batch	integer

Table .8: Parameter Settings Explanations

2. Data Content Description

In this Section, we provide the information data input format of this study, which is used as the data input format. They are given as follows.

FOD_ID	Global unique identifier
FIRE_NAME	Name of the incident, from the fire report (primary) or ICS-209 report (secondary).
date(julianday(DISCOVERY_DATE))	Date on which the fire was discovered or confirmed to exist
DISCOVERY_TIME	Time of day that the fire was discovered or confirmed to exist
STAT_CAUSE_CODE	Code for the (statistical) cause of the fire
STAT_CAUSE_DESCR	Description of the (statistical) cause of the fire
LATITUDE	Latitude (NAD83) for point location of the fire (decimal degrees)
LONGITUDE	Longitude (NAD83) for point location of the fire (decimal degrees).
FIRE_SIZE_CLASS	Code for fire size based on the number of acres within the final fire perimeter expenditures
FIRE_SIZE	Estimate of acres within the final perimeter of the fire

Table .9: FPA_FOD description[9]

3. General Wildfire Causes defined in National Wildfire Coordinating Group

In this Section, we list all known or defined causes of a wildfire in National Wildfire Coordinating Group (NWCG).

Table .10: Gernal Causes by National Wildfire Coordinating Group[61]

Existing NASF Cause Code	Proposed Fire Cause Standard
1-Lightning	Natural
2-Equipment Use	Equipment and vehicle use
3-Smoking	Smoking
4-Campfire	Recreation and ceremony
5-Debris Burning	Debris and open burning
6-Railroad	Railroad operations and maintenance
7-Arson	Arson
8-Children	Misuse of fire by a minor
9-Miscellaneous	Other causes
10-Fireworks	Fireworks
11- Power line	Power generation/transmission/distribution
12-Structure	Structure (under Other)
	Firearms and explosive use
	Undetermined (Human or Natural)

4. Vegetation Categories

In this Section, we provide a list of vegetation categories that are used in the present study, which is given as follow.

Vegetation	Dominant vegetation in the areas
1	Tropical Evergreen Broadleaf Forest
2	Tropical Deciduous Broadleaf Forest
3	Temperate Evergreen Broadleaf Forest
4	Temperate Evergreen Needleleaf Forest TmpENF
5	Temperate Deciduous Broadleaf Forest
6	Boreal Evergreen Needleleaf Forest
7	Boreal Deciduous Needleleaf Forest
8	Savanna
9	C3 Grassland/Steppe
10	C4 Grassland/Steppe
11	Dense Shrubland
12	Open Shrubland
13	Tundra Tundra
14	Desert
15	Polar Desert/Rock/Ice
16	Secondary Tropical Evergreen Broadleaf Forest
17	Secondary Tropical Deciduous Broadleaf Forest
18	Secondary Temperate Evergreen Broadleaf Forest
19	Secondary Temperate Evergreen Needleleaf Forest
20	Secondary Temperate Deciduous Broadleaf Forest
21	Secondary Boreal Evergreen Needleleaf Forest
22	Secondary Boreal Deciduous Needleleaf Forest
23	Water/Rivers Water
24	C3 Cropland
25	C4 Cropland
26	C3 Pastureland
27	C4 Pastureland, 28:Urban land

Table .11: Vegetation Categories

5. Synthetic Minority Over-sampling Technique(SMOTE)

In this Section, we briefly outline the Synthetic Minority Over-sampling Algorithm as follows.

Algorithm 1 Synthetic Minority Over-sampling Technique (SMOTE)[24]

Calculate Euclidean Distance between every samples with minorities S_{min} to find $k - nearest$
Find N , based on proportion of minorities and majorities, for each minority sample X , randomly choosing from its nearest sample X_n
for each X_n **do** $X_{new} = X + random(0, 1) \times |X - X_n|$
end for

6. Precision

In this Section, based on the conditional probability of a random event, we provide a mathematical formula to calculate the precision of the developed high-resolution Bayesian learning neural network model, which is given as follows.

$$\begin{aligned} Precision &= \mathbb{P}(actual = 1 | predict = 1) \\ &= \frac{\mathbb{P}(actual = 1, predict = 1)}{\mathbb{P}(predict = 1)} \\ &= \frac{\mathbb{P}(predict = 1 | actual = 1) \mathbb{P}(actual = 1)}{\mathbb{P}(predict = 1, actual = 1) + \mathbb{P}(predict = 1, actual = 0)} \\ &= \frac{\mathbb{P}(predict = 1 | actual = 1) \mathbb{P}(actual = 1)}{\mathbb{P}(predict = 1 | actual = 1) \mathbb{P}(actual = 1) + \mathbb{P}(predict = 1 | actual = 0) \mathbb{P}(actual = 0)} \\ &= \frac{TPR \cdot n}{TPR \cdot n + FPR \cdot (1 - n)} \end{aligned}$$

where n is the proportion of the actual true. Based on the equation above, precision is related to the proportion of true and false data, once the $\frac{FPR}{TPR}$ is fixed, it increases with n increases. However, TPR and FPR are not related to the proportion of the data, since $TPR = \mathbb{P}(predict = 1 | actual = 1)$ and $FPR = \mathbb{P}(predict = 1 | actual = 0)$ [50].

7. Example of Sample Outputs

In this Section, we show an example of sample outputs. Figure .28 displays the sample outputs of the image No. 1333.

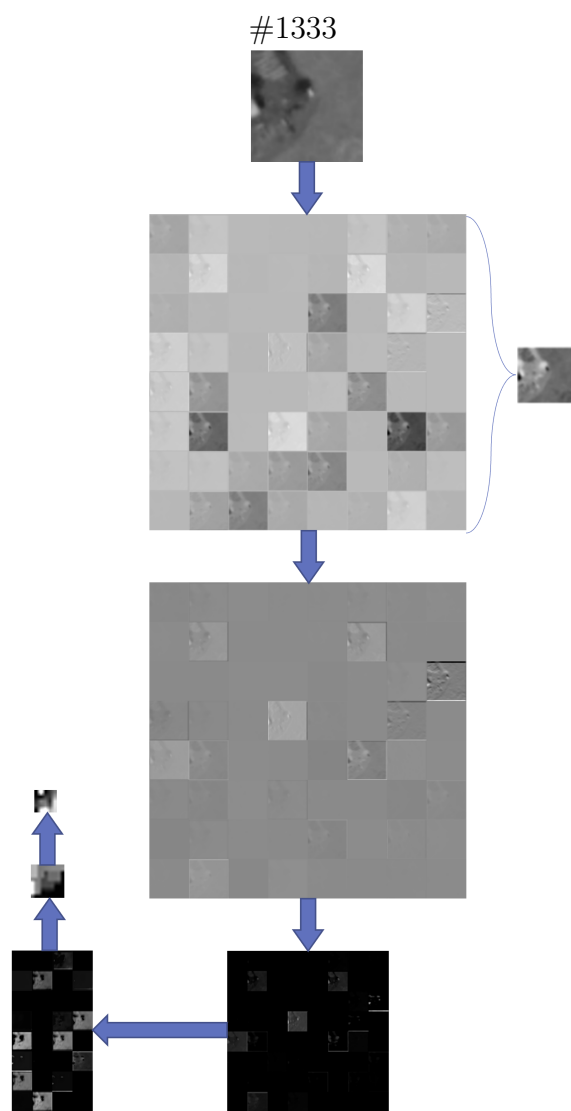


Figure .28: Image flow of image #1333 for each layer. From top: original input → 1st convolution output → 1st batch normalization output → 1st maxpooling output → 1st residual block output → WIT output